

HASP 2019 Final Flight and Science Report

Silicon Photomultiplier Array for Capturing Energetic Radiation

Louisiana State University

Blaine H Irle, Aaron Ryan, Emma Western
December 13, 2019

Table of Contents

1. Abstract.....	3
2. Background.....	4
3. Mission Statement.....	5
4. Mission Objectives.....	5
5. Context.....	5
6. Principle of Operation.....	7
7. Design & Fabrication.....	9
7.1 Mechanical Systems.....	9
7.1.1 BGO-SiPM Detector Unit.....	9
7.1.2 Payload Housing.....	9
7.1.3 Inner Payload.....	10
7.2 Electrical Systems.....	12
7.2.1 SiPM End Board.....	12
7.2.2 Payload Microcontrollers.....	12
7.2.3 Flight Controller Shield.....	12
7.2.4 Data Recorder Shield.....	13
7.2.5 Calibration of Temperature Sensors.....	14
7.2.6 Calibration of Voltage Monitors.....	16
7.3 Software Systems.....	17
7.3.1 Flight Controller Software.....	17
7.3.2 Flight Controller Data Management.....	17
7.3.3 Data Recorder Software.....	17
8. Test Flight.....	19
9. Integration.....	21
10. HASP Pre-Flight Operations.....	22
11. HASP Flight.....	23
12. Results.....	24
12.1 Overnight Run.....	24
12.2 Flight.....	28
13. Demographic.....	38
14. Publications.....	39
15. References.....	40
16. Appendices.....	41

1. Abstract

Storm systems can produce highly energetic gamma ray emissions of energies up to 10s of MeVs. These terrestrial gamma-ray flashes (TGFs) have been observed by satellite and ground-based detectors. This report overviews the design, testing, flight and flight results of a gamma ray detector (SPACER) suitable for observing these TGFs from the balloon altitudes closer to the suspected source locations above storm systems at high altitudes. The goal of SPACER is to be able detect emissions of gamma rays from a TGF at lateral distances of 10s of km with a ms time resolution. This detector is capable of measuring gamma ray count rates on millisecond time bin intervals from 8 bismuth germanate (BGO) scintillators using silicon photomultipliers (SiPMs). The detector was flown as a large payload aboard the High-Altitude Student Payload (HASP) platform on September 5th, 2019. With exception to two power cycles, SPACER remained functional throughout flight and was able to record environmental and SIPM count data. From this flight data a proof of concept and a baseline of the detector's performance was able to be established.

2. Background

High energy gamma-rays are typically thought to come from extraterrestrial sources or manmade sources such as nuclear weapons or reactors. However, similar energy emissions, called terrestrial gamma-ray flashes (TGFs) appear to be associated with thunderstorm lightning strikes. TGFs pose a risk of radiation exposure to people and damage to equipment due their close proximity to the ground and how widespread and frequent lightning strikes are. However, not every lightning strike creates a gamma ray flash.

TGFs were first observed by the Burst and Transient Source Experiment (BATSE) aboard the Compton Gamma Ray observatory in 1994 [Fishman et al., 1994]. BATSE's intended observation target was cosmic ray gamma-ray bursts. BATSE was equipped with NaI scintillators in each of the 8 corners of the space craft, so it was sensitive to x-ray and gamma-ray emissions from the whole sky. Four of the BATSE detectors were always facing down towards the Earth. Flashes were observed coming from regions of storm activity with time scales on the order milliseconds, which is similar to the observed time scale of electrical disturbances and optical emissions associated with lightning strikes. Additional research on these emissions have been made by space-based instruments (RHESSI, AGILE, Gamm-ray Burst Monitor, and Fermi Large Area Telescope), ground-based instruments (TETRA and Aragats Space Environment Center), and aircraft borne instruments (Airborne Detector for Energetic Lightning Emissions).

There are two main models for explaining how a TGF can occur. When a sufficiently strong electric field exists within air, the rate at which electrons gain energy will exceed the rate that they lose energy through bremsstrahlung and ionization. As these electrons ionize the air additional free electrons are produced that are then themselves accelerated leading to an avalanche of energetic electrons. This is known as the relativistic runaway electron avalanche (RREA) mechanism. With a sufficiently strong electric field, even thermally excited electrons are capable of being accelerated into a RREA. One possible model is that high electric fields in lightning leaders at the tip of lightning can initiate a RREA. The magnitude of electric fields in leaders observed near the ground are insufficient to produce a RREA, but it has been proposed that the potential differences are greater in the clouds. Also, Monte-Carlo simulations of this model produce a steeper high-end spectrum than observed. Another proposed model involves a feedback loop of positrons from pair production and backscattered x-rays that generate additional runaway electrons. This is known as a relativistic feedback discharge (RFD) [Dwyer et al., 2013].

Atmospheric attenuation is expected to significantly decrease photon flux as distance from the source increases. Because of this, it is suspected only a portion of the most luminous events have been observed. Detected gamma-rays have had energies up to the order of 100 MeV [Dwyer et al., 2012], leading to an attenuation length of several kilometers at these energies. At energies in excess of 10 MeV, the gamma-ray flux is several orders of magnitude below those at lower energies. The timescale of these events is on the order of sub-milliseconds, which is similar to the observed time scale of electrical disturbances and optical emissions associated with lightning strikes [Dwyer et al., 2012] Airborne observations [Dwyer et al., 2012] of nearby storm

systems detected only a single emission out of 1000 discharge events that occurred within 10 km of the aircraft. These observations lead to estimates of TGFs occurring in 0.1-1% of lightning flashes. Given the low statistics, further work studying TGFs in situ will be of great use in determining the gamma yield for lightning strikes.

3. Mission Statement

SPACER will monitor the atmospheric gamma-ray flux in environments and on timescales associated with Terrestrial Gamma-Ray Flashes. HASP flight will establish a proof of concept as well as a baseline of SPACER's performance.

4. Mission Objectives

1. Measure and record the gamma-ray flux in the atmosphere with a detector.
2. Measure the gamma-ray flux on millisecond timescales with the detector.
3. Monitor and record environmental factors that may affect the detector's performance.
4. Timestamp recorded data to allow for coordination with electromagnetic measurements post-flight.
5. Establish the performance of SPACER at background.
6. Survive the environmental stresses of space flight.

5. Context

Silicon Photomultiplier Array for Capturing Energy Radiation (SPACER) is a continuation of a payload originally designed for Correlation of Terrestrial gamma-ray flashes, Electric Fields, and Lightning strikes (COTEL). The gamma-ray detector's purpose was to detect gamma-rays created inside thunderstorms by employing a bismuth germinate (BGO) crystal and silicon photomultipliers (SiPMs). Figure 1 shows the final set-up of the COTEL gamma-ray detector as of summer 2018. Graduate and undergraduate students worked on the payload during the summer, which resulted in one test flight. The payload successfully detected cosmic rays during lab testing, however the flight resulted in no detections. Upon analysis, it was found the mechanical interface between the SiPMs and the crystal was poor. Lab testing and postflight analysis also revealed a difference in the elapsed time according to the GPS and MHz oscillator, with discrepancies greater than 65 ms during each read. The OS of the payload's flight computer, Raspberry Pi, prioritized internal operations over reading the data counters resulting in overflowing counters and the risk of lost counts.

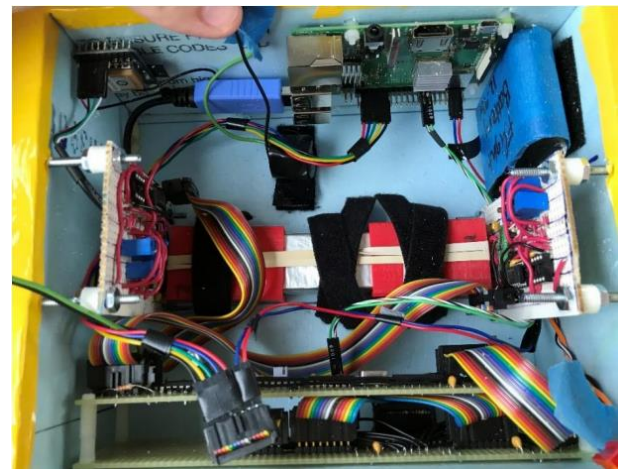


Figure 1: Fully assembled COTEL payload that was flown in the summer of 2018

6. Principle of Operation

The payload is designed around a BGO crystal and Silicon Photomultiplier. Due to the relatively heavy nuclei in the BGO crystal, gamma-rays will induce pair production that will in turn induce the production of fluorescence photons. BGO has a photon yield of ~8-10 photons/KeV with emission spectrum peaking at 480 nm. This emitted spectrum lays within the detectable region of light that SiPMs are capable of detecting. BGO crystals lack the requirement for high voltages or pressurized chambers that other gamma detectors such as Geiger counters and Photo Multiplier Tubes require, making a SiPM – BGO crystal array an ideal choice for a balloon flight.

SiPMs are integrated circuits that mimic the functionality of traditional photomultiplier tubes (PMTs). A SiPM is an array (ranging from 100 to several 1000 per mm²) of small photodiodes with a small resistor. When a photon is absorbed in the diode, a current is produced that is rapidly quenched by the resistor allowing the diode to return to its initial state. Each individual photodiode has an on or off state but by combining several diodes in a large array and combining their output, proportional information about the total amount of light absorbed can be obtained. Like PMTs, SiPMs are capable of detecting single photon events but have a few advantages over a PMTs. SiPMs operate at a much lower voltage compared to the many 100s of volts necessary to operate a PMT. Additionally, SiPMs are solid state devices and are less sensitive to external magnetic fields and mechanical shock.

The BGO crystals were recycled by the SPACER team from a previous cosmic ray experiment at LSU called ATIC that utilized an array of these crystals to measure the cosmic ray flux of the atmosphere [Wefel & Guzik, 2001]. Particles of sufficient energy that interact with the crystal produce photons in the crystal that are detected by SENSIL Silicon Photomultipliers placed at both ends of the crystal. These SiPMs are soldered onto custom printed circuit boards (PCB), hereby referred to as SiPM endboards, and operate at a bias voltage of 27.5V. Photons produced by the BGO crystal are amplified by the SiPMs and converted into a 1-5V electrical pulse that is sent to the payload's readout electronics. The readout electronics of SPACER convert the signal into a logic pulse that is sent to a register on a 16-bit counter. Each SiPM in the payload has an associated register on a 16-bit counter. These registers are read out approximately once every millisecond and recorded to onboard memory by one of the payload's microcontrollers (Arduino Due). There are three microcontrollers onboard SPACER, and the two responsible for recording and storing count information from the readout electronics will hereby be referred to as Data Recorders.

In total, SPACER consists of 8 BGO crystals and 16 SENSIL Silicon Photomultipliers. Each SiPM is given an optical pad to maintain good optical contact with the BGO crystal. The 16 SiPMs are divided into two groups, one for the left sides of the crystals and one for the right sides, each with their own readout electronics, Data Recorder, and SD card storage. In addition, each Data Recorder is responsible for reading a count register attached to a 1MHz oscillator. Electrical pulses from the 1 MHz oscillator are sent to the count register providing microsecond timescale information for the count data produced by the SiPM endboards. The Data Recorders are equipped with an Adafruit Logger Shields where they will store the count information.

Both Data Recorders communicate with another onboard microcontroller that functions as a payload Flight Controller (Arduino Due). The Flight Controller is responsible for communicating with HASP telemetry and executing any uplink commands. Environmental data, including payload altitude, payload temperature, SiPM bias voltage, and the output of the payload's main regulator, is monitored by the Flight Controller. Every five seconds the Flight Controller polls the Data Recorders for rough count data and stores this information along with the environmental data to onboard memory. This information is then sent to the ground station using HASP telemetry every five seconds.

7. Design & Fabrication

7.1 Mechanical Systems

7.1.1 BGO-SiPM Detector Unit

Because poor optical mating of the SiPM and BGO crystal was the cause of SPACER's previous iteration failing, it was important to ensure that the SiPM and BGO crystal remained in good optical contact throughout the entire flight. Previous versions of the BGO-SiPM detector unit utilized 3-D printed endcaps that were fitted onto both sides of the crystals. However, there were two issues with the endcaps that were revealed during the flight of Summer 2018. The first issues being that the material used to print the 3D endcaps warped during flight. This was due to the fill factor of the endcaps being too low while being printed as well as the walls of the endcap not being thick enough.

The second issue was although the endcaps fit snugly over the BGO crystal, there was no means of applying pressure to ensure that the SiPM and BGO crystal remained in solid optical contact throughout the flight. The team previously attempted to remedy this issue by putting rubber bands around both endcaps (see figure 1). This method did not work and led to the SiPM's being saturated by ambient light during flight.

To fix the first issue the SPACER team increased the fill factor of the endcaps when 3D printed as well as increased the thickness of the walls of the endcap itself. To ensure the endcaps kept the BGO and SiPM in optical contact with each other, an eyebolt was added to both sides of each endcap (figure 2). A spring was then hooked onto the eye of a bolt on one endcap and then hooked onto the eye of the bolt on another endcap, providing pressure for the BGO-SiPM joint. A collar to prevent stress on the crystal was also printed to slide over the middle of the crystal (figure 2).

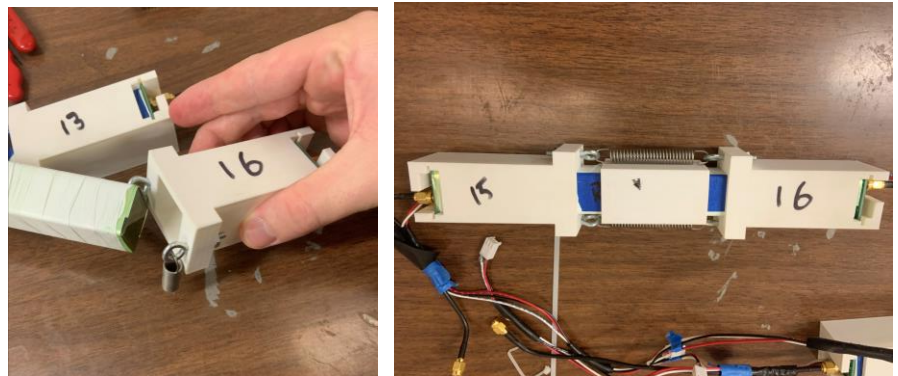


Figure 2: A BGO crystal being inserted into an endcap (left) and a fully-assembled BGO-SiPM detector unit (right).

7.1.2 Payload Housing

The structure that houses the SPACER payload needed to provide two main functions for flight. First, the housing needed to make sure the BGO-SiPM detector units as well as all electronics were secure and would survive any mechanical stress encountered during flight. Second, the housing needed to be light-tight so that ambient light would not saturate the detector. The SPACER payload frame is constructed using aluminum T-slot framing and is secured at its corners using aluminum corner braces and accompanying fastener. The payload frame's

dimensions measure 14.75" x 7.25" x 8.5". The payload is fitted with five separate walls, four for the sides and one for the top. The walls are a polished aluminum sheets, the polished side faces inward, acting as a IR reflector to help the payload reach a temperature equilibrium, while the dull side faces outward and is given a white powder coat finish to reduce solar heat absorption. Insulating compressible foam is then added to the walls' edges to prevent light leaks. The walls are secured directly to the payload using aluminum corner surface brackets and steel hex head screws as fasteners. The payload is then secured directly to the HASP mounting plate.

7.1.3 Inner Payload

Inside the frame the payload is divided into four bays with floors that are hereby referred to as bay plates. The bays are made of the same aluminum sheeting used for the payload walls. The first bay is made of an aluminum sheet that rests on the aluminum framing on the bottom of the payload and has dimensions 14.75" x 7.25" with cuts made at the corners to allow space for the corners of the payload

frame (figure 3). Rubber matting is applied on both sides of the aluminum sheeting to reduce mechanical stress/shock on the crystals during flight. The bay houses three BGO-SiPM detector units side-by-side (figure 3). These detector units are separated using 3-D printed spacers that also prevent lateral movement of the detector units during flight. Each spacer is secured to the bay

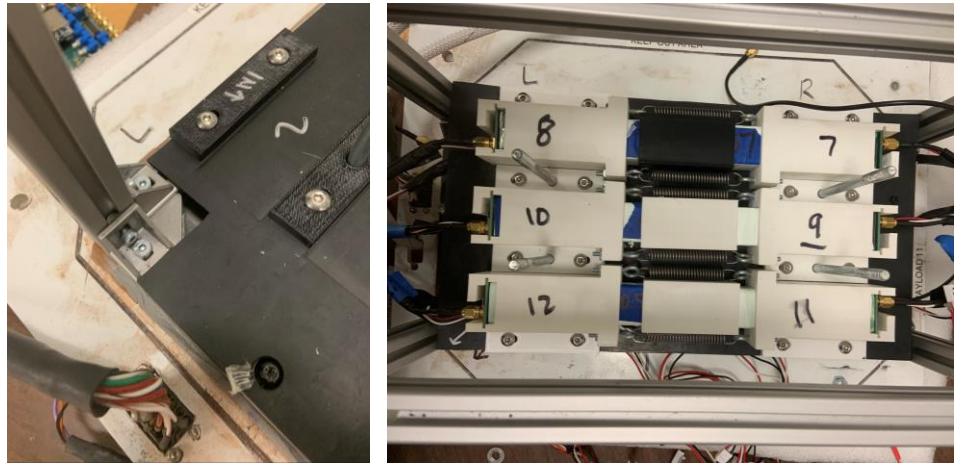


Figure 3: The first bay plate with 3-D printed spacers attached and cuts made for the payload frame (left) and a fully assembled payload bay housing three detector units (right).

using two steel button head hex drive screws. The second bay is almost identical to the first bay except its length is 13.25", this reduced length is to give clearance for the signal and power cables that run to each SiPM endboard (figure 4). The third bay is similar to the second bay except that it only houses two detector units, where the middle one has been removed. Another aluminum plate 13.25" x 7.25" with rubber matting on its bottom side is placed on top of the crystals in the third bay. Four bolts extend up through the HASP mounting plate and through the bottom of the payload, the bolts are then passed through the four holes in each of the bays (figure 4). Once the bays have been mounted a washer, locking washer, and nut are placed on each bolt and tightened until that payload bays are vertically secure. This compression reduces the mechanical shock as well as prevents the lateral movement the detector units experience during flight.

The fourth bay is then mounted on these bolts. The fourth bay is the electronics bay whose dimensions are 13.5" x 6.75". The electronics bay houses the payloads three microcontrollers and their respective shields, forming three electronics stacks. Each of these stacks are mounted to the bay plate with nylon standoffs to elevate them off the plates metallic surface.

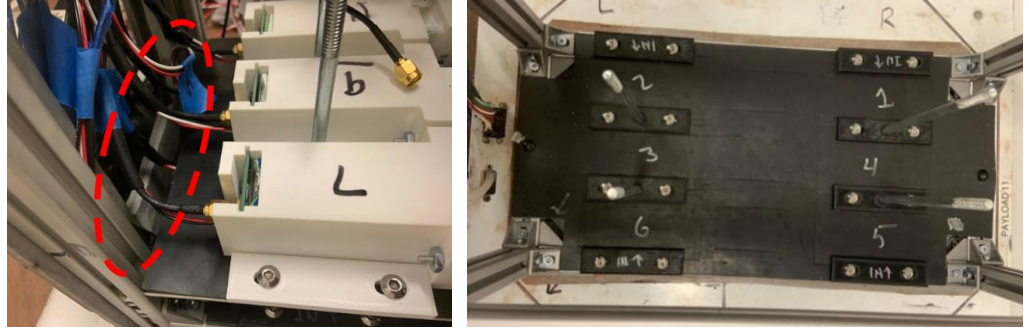


Figure 4: The second bay plate with its end shortened to allow for clearance of wires below(left) and the bottom bay plate with the four mounting bolts extending through (right).

7.2 Electrical Systems

7.2.1 SiPM Endboard

The SiPM endboard (Appendix A) contains two main circuit components. The first is a simple low pass filter that filters the SiPM bias voltage supply. The goal of this filter is to remove any ripple noise from the boost regulator as well as any line noise picked up from transmission from the bias source on the flight controller board to its supply point on the endboard. The second circuit is a transimpedance amplifying circuit that integrates the current pulse created when a photo-avalanche occurs in the SiPM generates a pulse $\sim 1\text{-}5\text{V}$. This pulse is transmitted through a shielded R-SMA connection to the readout electronics circuits.

7.2.2 Payload Microcontrollers

All microcontrollers used in SPACER are Arduino Dues. The Arduino line of microcontrollers was chosen after previous tries with Raspberry Pi's resulted in operating system interrupts stopping the payload software to manage background tasks, resulting in gaps during data collection. The Due model was chosen for its robustness as well as its superior 84 MHz clock speed and 512 kB of flash memory. Separate electronics shields were designed for the Flight Controller and Data Recorders and are attached directly to the microcontrollers.

7.2.3 Flight Controller Shield

A custom shield was made for the payload's Flight Controller microcontroller. The Flight Controller shield fulfilled three main functions: power management and distribution, handling payload communications, and environmental monitoring of the payload. The Flight Controller shield was powered off the 30V line of HASP power. The 30V line of HASP is immediately stepped down to 12V using a MHB75 DC-DC converter. This 12V line powers the Flight Controller and is delivered to the other shields for power. The shield then uses a MAX 16904 and MAX 16903 switching converters to step down the 12V to 5V and 3.3V respectively. The 5V line will power the amplifying circuit of the SiPM endboards. The 3.3V line will power the payload's temperature sensors and RS232-TTL level-shifter that facilitates communication between HASP telemetry and the Flight Controller. Lastly the shield uses two LT3461A boost regulators to step

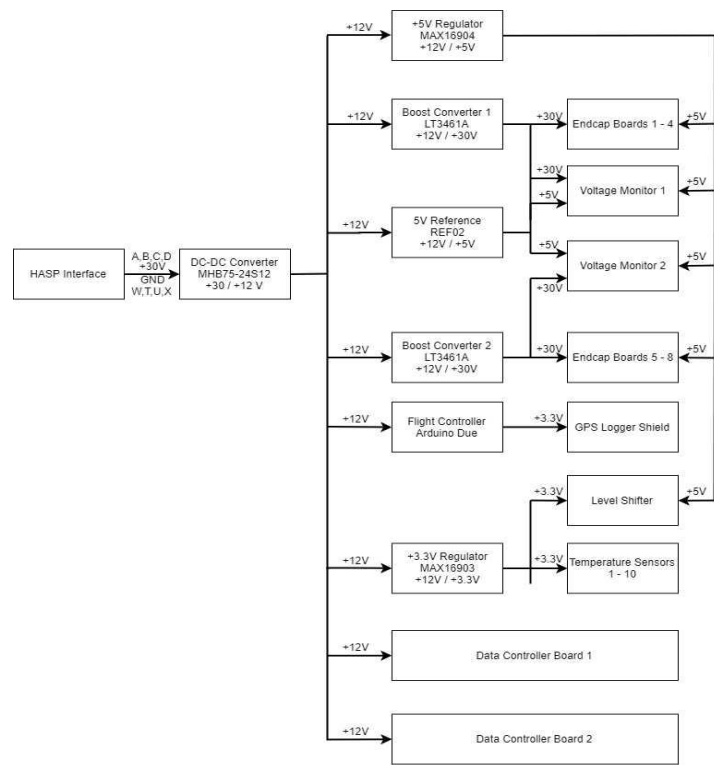


Figure 5: A power distribution diagram of the SPACER payload

up the 12V to 27V. Each boost regulator is responsible for providing the bias voltage for a bank of eight SiPMs (figure 5).

The Flight Controller shield is connected to HASP telemetry using a DB9 connection. The RS232 protocol from HASP is then sent through a RS232 -TTL level-shifter that enables communication with the Flight Controller. The Flight Controller shield also facilitates communication between the Flight Controller and Data Recorders. This is done via a separate comms bus for each Data Recorder that connects the shield to each Data Recorder shield. The comms bus has a TX and RX line that allows for UART serial communications between the microcontrollers, as well as a GPS PPS, 12V, and ground line. When the Flight Controller polls a Data Recorder for rough count data or executes a command, it does so via the TX/RX lines of the comms bus. For a full wiring table and diagram for SPACER see Appendix D.

The Flight Controller shield is equipped with 9 TMP36 temperature sensors that are powered off the 3.3V line with a functional performance from $-40\text{ }^{\circ}\text{C}$ - $+125\text{ }^{\circ}\text{C}$. These sensors are transistors that output a variable voltage from 0.5V to V_{cc} that is linearly proportional to the temperature of the sensor. The output of these sensors is then fed to one of the analog pins on the Flight Controller. The voltage on these pins is fed through the Flight Controller's ADC and then converted to a voltage using the team's calibration of the temperature sensors. The Flight Controller's ADC range is 0V-3.3V hence the sensors being powered off the 3.3V line. Three simple voltage divider circuits also monitor the output of the main DC-DC converter as well as the two boost regulators. The output of each of these circuits is connected to an analog pin on the microcontroller, and, just like the temperature sensors, is fed through the Flight Controllers ADC and converted into a voltage using the team's calibration of the voltage monitoring circuits.

The Flight Controller shield has an additional shield, Adafruit Ultimate GPS logger shield, mounted on top of it. The Ultimate GPS logger shield is powered off the 3.3V line of the Flight Controller and is responsible for providing the payload with GPS information such as GPS time, GPS coordinates, and altitude. The GPS module is equipped with an external antenna that is placed on the outside of the payload housing to maintain a GPS fix during flight. These values generated by the GPS are recorded by the flight controller and written with the rough count data. This data is stored to onboard memory to an SD card on the logger shield.

7.2.4 Data Recorder Shield

The Data Recorder Shield is responsible for converting the electrical signals of the SiPMs to count data to be read out by the Data Recorder, as well as provide fine timescale data for the counts. The Data Recorded shield is powered of the 12V line of the comms bus from the Flight Controller shield, and the 12V line is stepped down to 5V and 3.3V as it was on the Flight

Controller shield. The 5V line will power the shield's counter threshold circuit and the 3.3V line will power the shields counting circuits and I2C interface circuits (figure 6).

Each Data Recorder shield is connected to 8 SiPMs via a shielded R-SMA cable. The shield is equipped with two MAX 908E quad comparators. These comparators are low voltage, high-speed comparators that operate on 5V. The signals from the SiPMs are sent to the comparators and compared to an adjustable threshold. This adjustable threshold ranges from 0-5V and is the output of a simple voltage dividing circuit made with a 100k potentiometer. If the signal generated by the SiPM exceeds this threshold a 5V logic pulse is created. This logic pulse is fed into a CD4504 level shifter that shifts the pulse down to 3.3V. This logic pulse is then sent to the register on a SN74LV8154 16-bit counter that is associated with that SiPM. The logic pulse causes the register of the counter to increment by one. The registers of these counters are connected to a PCF-8575C 16-bit I/O expander for I2C communications. This I/O expander allows the registers of the counters to be read out by the Data Recorder over I2C approximately once every millisecond (figure 7).

The Data Recorder shield also has a MXO45HST 1 MHz oscillator that operates at 5V. The oscillator generates electrical pulses every microsecond that is sent to a register of a 16-bit counter. The rollover pin of this register on the 16-bit counter is tied to an interrupt pin on the Data Recorder as a means of creating a 32-bit counter that stores microsecond timescale information of the count data. These 1 MHz oscillator registers are read out approximately once every millisecond by the data recorder along with the other count registers.

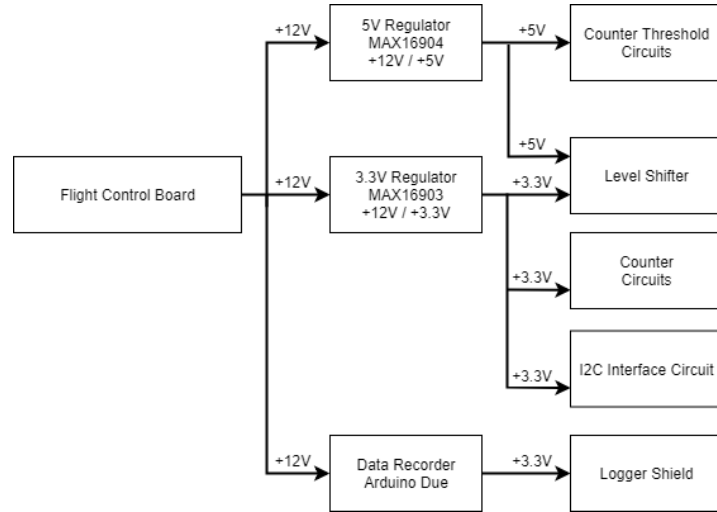


Figure 6: A power distribution diagram for the SPACER Flight Controller shield

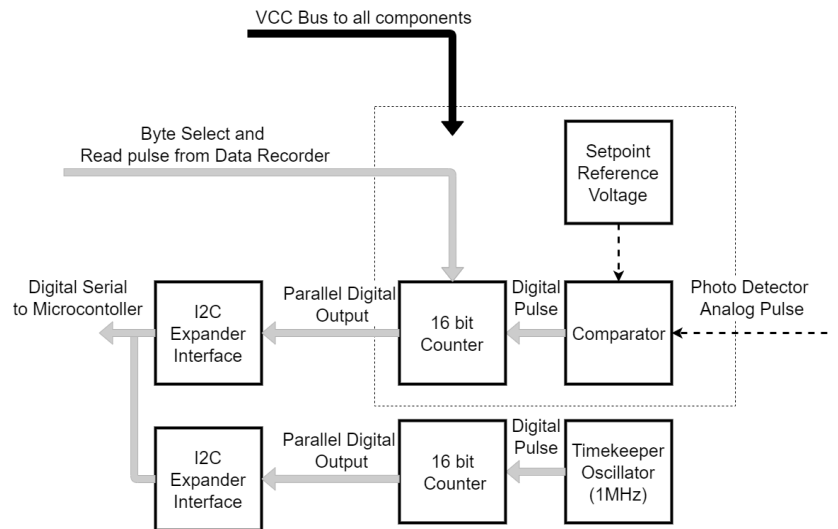


Figure 7: A system diagram of the SPACER Data Recorder Shield

7.2.5 Calibration of Temperature Sensors

Since the light yield of the BGO crystal is inversely proportional to the temperature of the crystal, it is important that the temperatures of the crystals are monitored throughout flight. As

noted, before, the Flight Controller shield is equipped with 9 TMP36 temperature sensors that have a functional range from -40°C - $+125^{\circ}\text{C}$. These sensors are transistors that output a variable voltage from 0.5V to V_{cc} that is linearly proportional to the temperature of the sensor. The outputs of these sensors are sent to analog pins on the Flight Controller. The voltages on these pins are sent to a 10-bit ADC that gives it a digital value. The ADC values needed to be calibrated to the temperatures SPACER would experience during HASP flight.

A simple three-point calibration was done on each sensor. The sensors were kept in a freezer and were left long enough to come into thermal equilibrium with the -27°C cooler. The ADC output of these sensors were then read 1000 times by the microcontroller and averaged. The same collection method was repeated for room temperature air at 23°C and a warm water bath at 73°C . These three points were then plotted for each sensor and given a calibration using a linear fit as seen in figure 8 for temperature sensor TMP1. For the calibrations for all the SPACER temperature sensor see Appendix E.

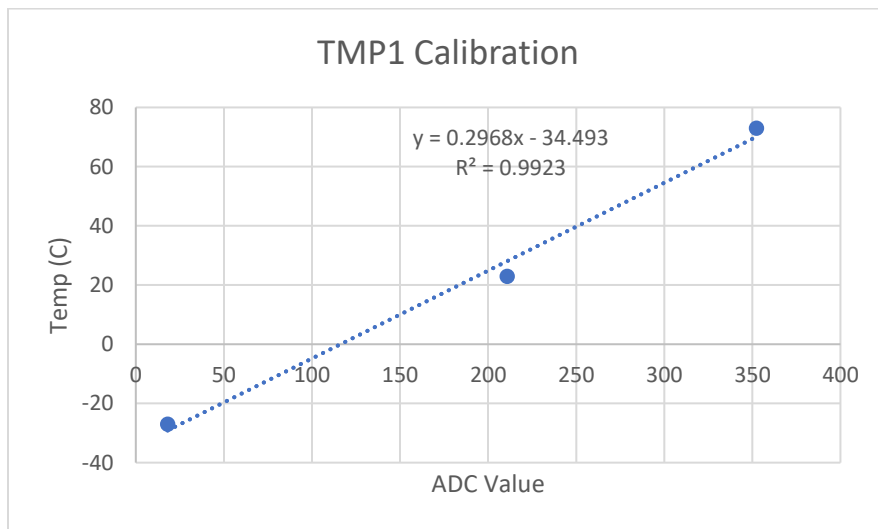


Figure 8: The data used for the temperature calibration of temperature sensor TMP 1 as well as the calibration equation

7.2.6 Calibration of Voltage Monitors

Because the gain of SiPMs is affected by the bias voltage provided to that SiPM, it was important that the bias voltage provided to both the SiPM banks be monitored throughout HASP flight. The bias voltage of the SiPM banks can be adjusted via a potentiometer in the boost regulator circuits and ranges from a value of 24V to approximately 30V. The bias voltage is scaled to the operational range of the Flight Controller's ADC using an AD822 op-amp. The bias voltage was first set to 24V and the flight controller collected the ADC values at this voltage 1000 times and averaged the values. The voltage was then increased by 0.5V and the same collection process was repeated. This process was repeated until a bias voltage of 29.5 V was reached. These values were then plotted and given a calibration using a linear fit as seen in figure 9.

The 12V MHB75 DC-DC converter is responsible for delivering power to the rest of the payload, so it was important that the output of this converter was monitored in real time. The output of this converter was called to the operational range of the Flight Controller ADC with an AD822 op-amp similarly to how the SiPM bias voltage was scaled. This time a DC power supply was connected to the 12V line of the shield. The 12V line was set to approximately 11V and the output of the Flight Controller ADC was recorded 1000 times and averaged. The DC power supply was then increased by 0.5V and the same collection process was repeated again. This process was repeated until the DC power supply reached a voltage of 13V. These values were plotted and given a calibration using a linear fit as well, for the calibrations of all the voltage monitor circuits see Appendix E.

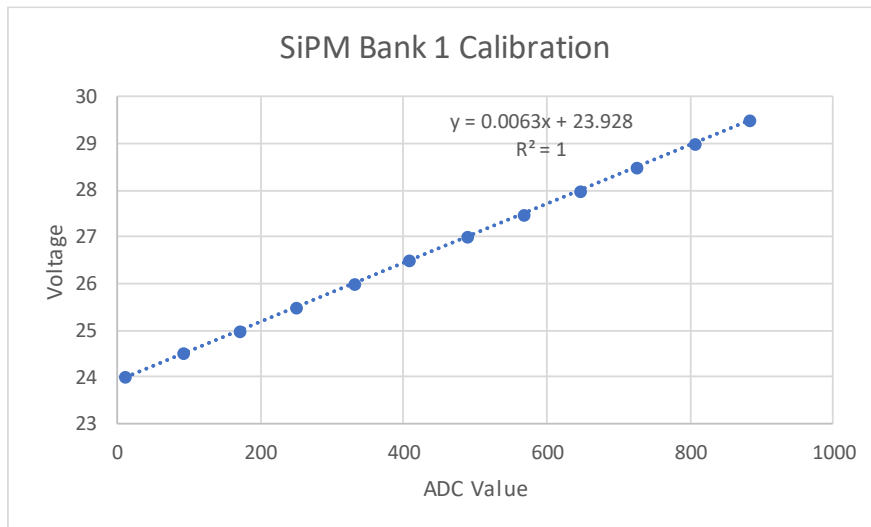


Figure 9: The data used for calibration of the voltage monitor circuit for SiPM bank 1 as well as the calibration equation

7.3 Software

7.3.1 Flight Controller Software

On power up the Flight Controller software begins by defining all global variables and setting up communications protocols then waits for any transient power behavior to subside. The software then continuously switches between checking the HASP telemetry serial port for a new uplink command and checking the GPS for a new NMEA string. If a command is received from HASP telemetry the software verifies that it is a valid command and sends a notice to HASP telemetry if not. If the command is valid the kind and time of the command received is stored. Depending on the type of command, it is then executed by the Flight Controller or sent to a Data Recorder to be executed. If a new NMEA string is received from the GPS serial port, the Flight Controller updates its timestamp and altitude; if the GPS does not have a fix, the Flight Controller assigns “No fix!” to the timestamp.

7.3.2 Flight Controller Data Management

The Flight Controller polls the Data Recorders for rough count data using a CreatePacket function that is executed by a 5-second interrupt disciplined by the GPS pulse-per-second signal. The CreatePacket function creates a data packet that will be stored to the Flight Controller’s SD card and sent to HASP telemetry for transmission to the ground station. The function begins the data packet with the timestamp, altitude, number of satellites, and fix quality from the last NMEA sting. It then concatenates the milliseconds since power on, last command received, and time of last command received to the data packet. The flight controller then reads the payload’s critical voltages (output of boost regulator circuits and main power regulator) and temperatures and concatenates them to the end of the data packet. The Flight Controller then polls Data Recorder One for a data packet and then Data Recorder Two for a data packet. The packets from the Data Recorders give the milliseconds since power up, current total counts of the 1 MHz oscillator and all the SiPMs, the last command received from the Flight Controller, and the status of that command. For a table detailing the contents of the Flight Controller data packet and an example please see Appendix F. The packets from the Data Recorders are concatenated to the end of the Flight Controller data packet which is then saved to the SD card and sent to HASP telemetry. Once the packet is sent, it is erased, and a counter is incremented by one. Once the counter reaches a value of 60, the file on the SD card is closed and a new one is created with the GPS timestamp used as the name.

7.3.3 Data Recorder Software

On power up the Data Recorder software begins by defining all global variables and setting up communications protocols then waits for any transient power behavior to subside. The software then reads all the counter values and appends the data to a String and checks if a command has been received from the Flight Controller. These two tasks loop repeatedly until the Arduino loses power. The speed at which these actions are performed means that the counters are read approximately every millisecond. Every time the counters are read, a

readCount variable is incremented by 1. Once this variable reaches 100, the data string is written to the SD card and the data string is reset to being empty. For an example of the data packet and its format please see Appendix G. A command from the Flight Controller contains three pieces of information: ID number, Flight Controller's current filename, and the command itself (2 bytes). The first byte of the command specifies the location the command is to be sent; the second byte of the command specifies what action is to be taken at that location. For a complete list of SPACER's commands and their functions please see Appendix H. Once received, the entire command is written to the SD card. The information is parsed to extract the actual command byte. The action corresponding to this byte's value is then taken. After the action has been performed, the Data Recorder sends an update to the Flight Controller. The Data Recorder's update to the Flight Controller includes: Data Recorder's uptime, counter values (including the MHz oscillator), last command received, result of the last command, an ignore String that acts as a flag for bad/noisy SiPMs, and the ID and Flight Controller filename corresponding to the last received command. This record update is sent to the Flight Controller every 5 seconds.

8. Test Flight

On June 6th, 2019 a scaled-down version of the SPACER payload was flown to test proof of concept of the BGO-SiPM detector, the readout electronics, and power distribution electronics. A single half-crystal detector unit was flown with an Arduino Due, a Flight Controller shield prototype, a Data Recorder shield prototype, and an Adafruit Ultimate GPS Logger Shield figure 10. The Arduino Due was loaded with a prototype code that combined the tasks of the Flight Controller and Data Recorder. The Due read out the count register of the SiPMs and 1MHz oscillator and GPS data from the Adafruit GPS module and stored it to the SD card on the logger shield. The SPACER payload was launched out of Churchpoint, LA at 15:45 UTC. The payload reached apogee of 90 kft at 17:06 UTC and immediately began descent. The payload touched down at 17:42 UTC for a total flight time of 117 minutes. The payload's flight profile can be seen in Appendix I.



Figure 10: Illustration of the assembly of the scaled-down SPACER payload flown on June 6th, 2019

The payload's power regulation and SiPM circuits functioned throughout the test flight. The team was able to observe the payload pass through the Pfostzer maximum, however multiple issues were discovered. The first issue discovered before the payload's launch was that ambient light was hitting the SiPMs causing them to saturate. This issue is something that had not come up when bench testing the detector in a dark box. After repeated efforts to fix the situation it was decided to wrap the whole BGO-SiPM detector unit in electrical tape to prevent saturation of the SiPMs. Reflective film from 3M used in the manufacture of LCD screens was purchased to fix this problem from occurring in the future. Each crystal was wrapped in the film with only the ends being exposed to the SiPM endboards. Insulating compressible foam was also added to the finished payload's walls to prevent ambient light from entering the payload.

The second issue discovered was that the counts of the SiPMs would increase and even decrease sporadically. The magnitude of these sporadic increases/decreases were always certain powers of 2. This issue was eventually attributed to multiple lifted pins on the 16-bit counter of the readout circuitry that were tied to powers of two.

The third issue involved multiple files created during the flight being corrupted and resulting in loss of data. This problem had been something the team had run into multiple times in the past where whole SD cards would get corrupted but could not be resolved before flight. After further testing it was discovered that the clock speed of the Arduino Due was too fast for

SPI communications as well as a poor connection to the SD card on the SPI pins, causing bits too flip in the file system. Once the clock speed was reduced and wires in the payload shortened, corruption of files was no longer an issue.

Something already known by the team but finally observed during the test flight is the BGO crystals' photon yield varying with temperature. This is something the team would need to correct for when SPACER is at float during HASP flight.

9. Integration

On July 17th, 2019 SPACER travelled to Palestine, Texas to participate in HASP integration. During the week of integration SPACER underwent two thermovac tests to test its operation in an environment similar to that experienced during space flight. During the first thermovac test, commands were sent to test having the data recorders ignore a noisy SiPM. When the command was executed by the Data Recorders the wrong SiPM would be ignored. The team discovered that this was an issue due to the indexing of the 'ignore' array for the Data Recorder beginning at zero instead of one. For a complete timeline of events for the first and second thermovac tests please see Appendix J.

It was observed that SiPM (1,2) on Data Recorder 1 was not counting during the thermovac tests, and SiPM (2,3) on Data Recorder 2 would intermittently stop counting. On multiple occasions during bench testing and during the first thermovac test Data Recorder 1's count registers would stop incrementing. To fix the problem power cycles were requested. Cycling the power fixed the problem, but SPACER would continue to sporadically stop counting. At first it was thought a light leak in the payload was causing the SiPMs to be saturated. Further testing after the thermovac test revealed that the shielded R-SMA cable connecting SiPM (2,3) to Data Recorder 2's shield had a short from signal to ground. This short caused the 5V regulator that the SiPM amplifier circuits use to stop working. A power cycle would make the 5V regulator begin to work again until there was another short in the cable. After the test, when SiPM (1,2) was exposed to direct light, its output did not read high. It was discovered that the SiPM's power cable had been severed. To prevent these problems from happening again all SiPM's signal cables were tested, and all SiPM power cables were hot glued at their bases to prevent bending stress.

During the first test some SiPMs were recording counts much faster than others. After the test the team made sure that the thresholds of the comparators for all the SiPM's were at the same value. The potentiometers were then hot glued into place to prevent the thresholds from changing. Further testing showed this solved SiPMs counting much faster than others, but differences in SiPM efficiencies remained that the team would need to correct for during flight.

During the second thermovac test, SPACER was functional then stopped receiving packets from the Data Recorders after 27 minutes. A power cycle was requested from the team 8 minutes later at 9:31 AM. Upon being started back up, SPACER was functional for one minute before no longer receiving packets from the Data Recorders. The team requested two more power cycles, but the problem persisted. The issue was because the team foolishly made changes to Data Recorder software after the first thermovac test. The team had tried to update how the Data Recorders write to their SD cards. When testing the update, the team set a limit to the number of files allowed on the SD card that allowed approximately 40 minutes of data to be written. After the second thermovac test, the previous functional code was downloaded on to the Data Recorders. After integration the team took SPACER back to Baton Rouge for further testing to verify that it was ready for HASP flight.

10. HASP Pre-flight Operations

SPACER arrived in Ft. Sumner, New Mexico full configured for HASP flight on August 8th 15:00:00 UTC. For a complete timeline of events from SPACER's arrival in Ft. Sumner, New Mexico through HASP flight please see Appendix K. At 16:30:00 SPACER was attached to the HASP gondola and test commands were sent using the HASP ground station. The data packet received from SPACER showed that some of the temperature sensors were connected. SPACER was powered down and taken off the HASP gondola the next day at 14:00:00 UTC. SPACER was taken apart so that all the temperature sensors could be connected and then put back into flight configuration and attached to the HASP gondola at 15:15:00 UTC.

The team then began an overnight run of SPACER at 15:19:00. The overnight run would establish a background for the detector performance at ground level. For results and a discussion of the data from the overnight run see section 12.2. The overnight run was concluded the next morning on 08/30/2019 14:24:04 UTC.

On 09/01/2019 15:30:40, SPACER participated in the HASP hang test until 16:41:23. The team requested a power cycle and sent commands that would be executed on each Data Recorder to confirm the payload's functionality.

11. HASP Flight

HASP flight took place on September 5th, 2019. The HASP gondola was powered up at 11:40:00 UTC time 01:23:15 before launch. The payload was able to telemeter data packets to the HASP ground station in the correct format. The data packets were able to confirm that the payload was functioning properly, and SPACER's GPS was able to get a fix. HASP launched at 13:03:15 UTC and began its ascent toward float. During ascent SPACER maintained functionality, however an issue with the temperature readings on the HASP power banks caused HASP to power down. HASP remained powered off during the end of ascent for 21 minutes from 15:13:00 UTC to 15:34:00 UTC. Once it was determined there were no issues with the HASP power banks, HASP was powered back up.

Upon powering up SPACER was no longer able to receive a GPS fix. During this time float began at 15:40:37 UTC. After not being able to receive a fix for over 30 minutes, the team decided to cycle SPACER's power in hopes of fixing the problem. SPACER was powered down at 16:11:43 UTC and remained powered off for 25 seconds until 16:12:08 UTC. The team decided at this point to just operate without a GPS fix as it was not mission critical. During descent SPACER's GPS module was again able to receive a fix. The SPACER team has flown the same GPS module on multiple balloon flights as well as lab testing with a GPS simulator and has confirmed the module's functionality at float altitudes.

Descent began at 23:17:56 UTC giving SPACER a float time of 07:37:19. HASP landed in Southeast Utah at 23:57:03 UTC for an entire flight time of 10:52:48. SPACER remained powered on and collected data for the whole flight with exception to the two power cycles. SPACER travelled back to Baton Rouge, Louisiana with the team where it was disassembled for post-flight analysis.

12. Results

12.1 Overnight Run

SPACER's overnight run in Ft. Sumner was over 23 hours long, but it was decided that the first three hours of the run were enough to establish a background for detector performance at ground level. The total counts of the SiPMs during the first three hours of the overnight run are plotted below with respect to time.

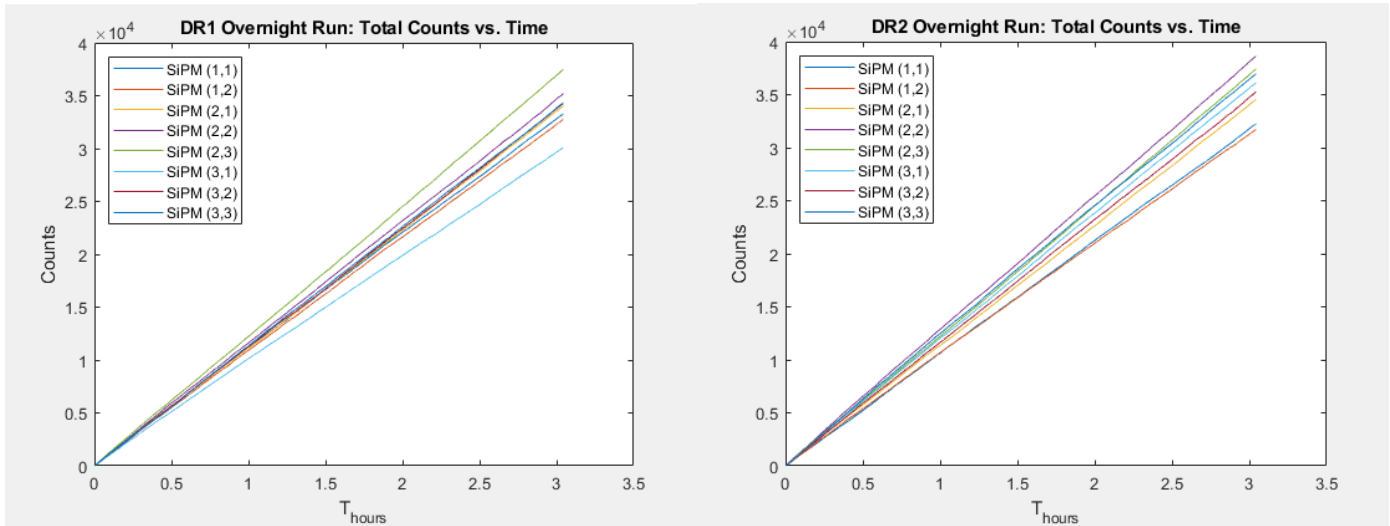


Figure 11: Plots of the SiPMs' total counts vs. time for the first three hours of the overnight run with $T=0$ at 08/29/2019 15:19:06 UTC

Because of variations in efficiency across different SiPMs, the counts from the overnight run needed to be normalized to a single reference SiPM. The measured counts of a SiPM would be multiplied by the ratio of the total counts of the reference SiPM to the total counts of the SiPM. The reference SiPM chosen was SiPM (2,2) on Data Recorder 1 and the equation for the normalization is shown below.

$$C_{\text{cor}} = C_{\text{meas}} * K_{\text{SiPM}}$$

$$K_{\text{SiPM}} = C_{\text{total(ref)}} / C_{\text{total}}$$

For a table of the normalization constant, K_{SiPM} , for each SiPM please see Appendix L. The total counts of the SiPMs with respect to time after the normalization can be seen in figure 12 below.

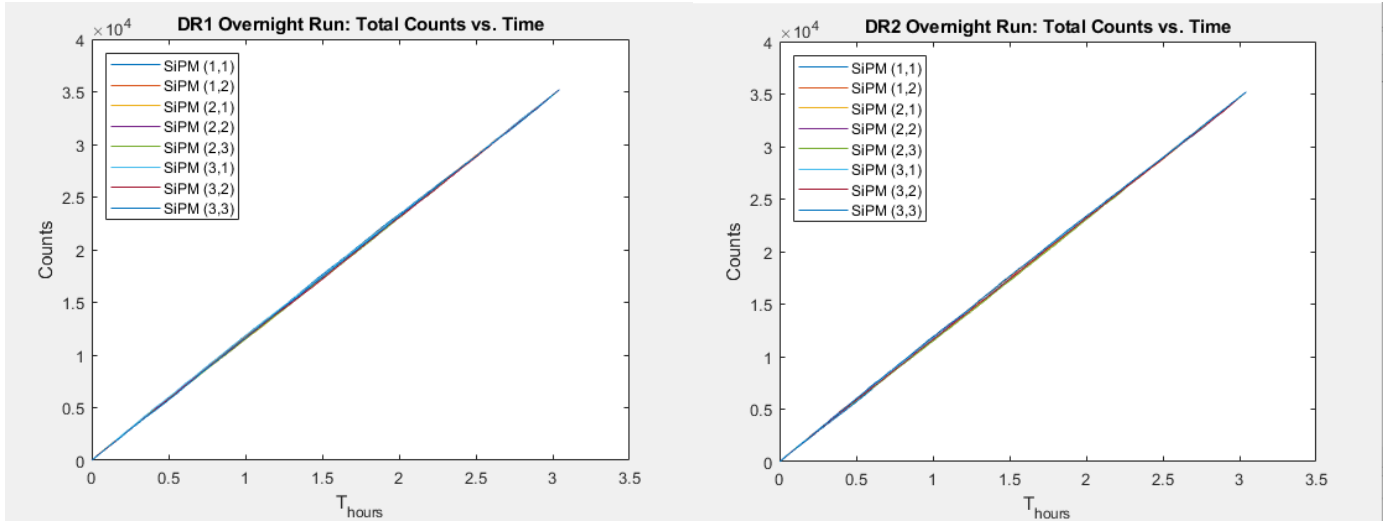


Figure 22: Plots of the SiPMs' normalized total counts vs. time for the first three hours of the overnight run with $T=0$ at 08/29/2019 15:19:06 UTC

Once the counts were normalized to a single SiPM, it was possible to look at the counters' count rates during the overnight run and compare their distributions. A plot of the normalized count rates with respect to time for crystal (1,2) during the overnight run are shown below.

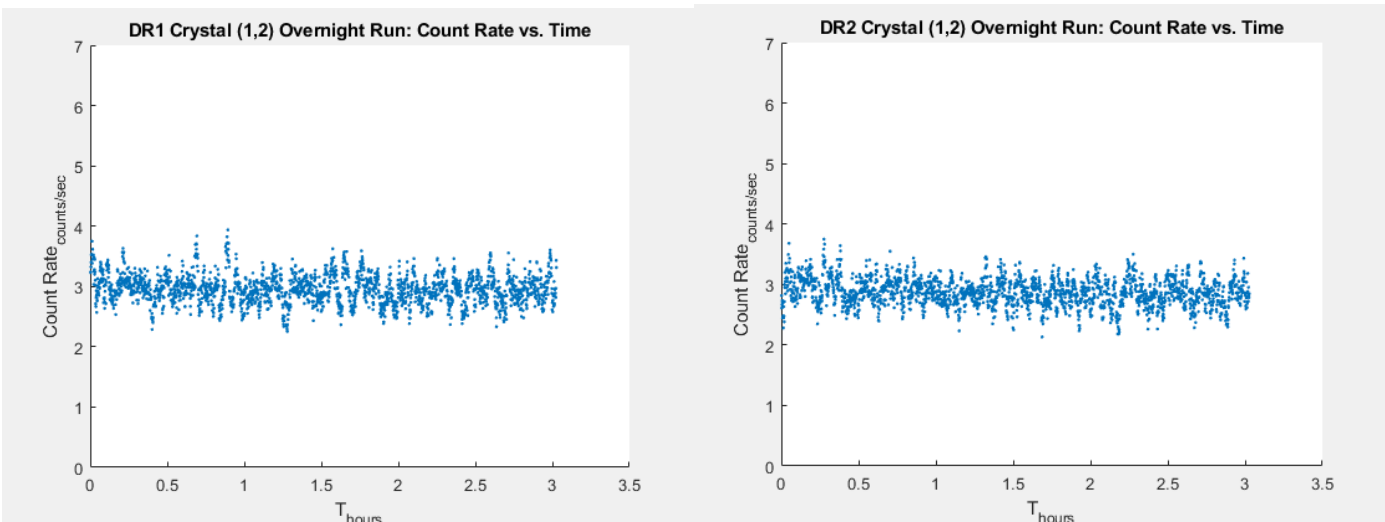


Figure 33: Plots of the normalized count rates vs. time for the SiPMs on crystal (1,2) during the first three hours of the overnight run with $T=0$ at 08/29/2019 15:19:06 UTC

To get a better idea of the behavior of the count rates of the SiPMs, distributions of their five-second averages for the overnight run were plotted and can be seen in figure 14.

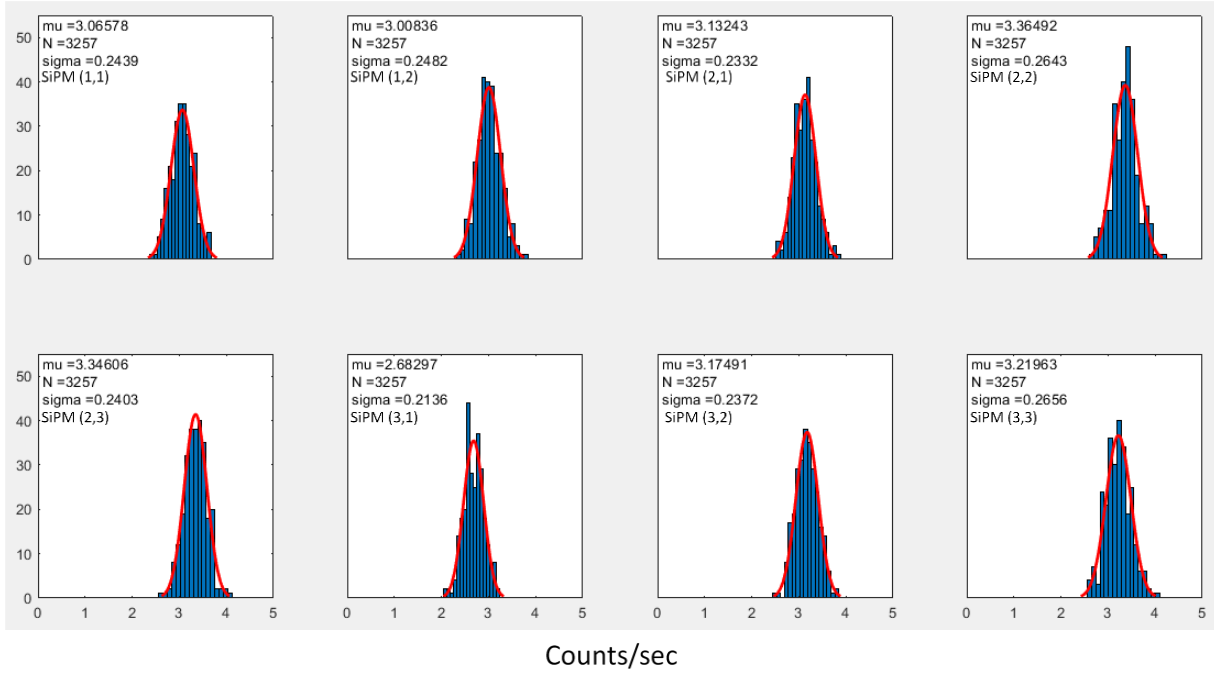


Figure 14: Plots of the distribution of the normalized SiPM count rates on Data Recorder 1 at ground-level during the overnight run.

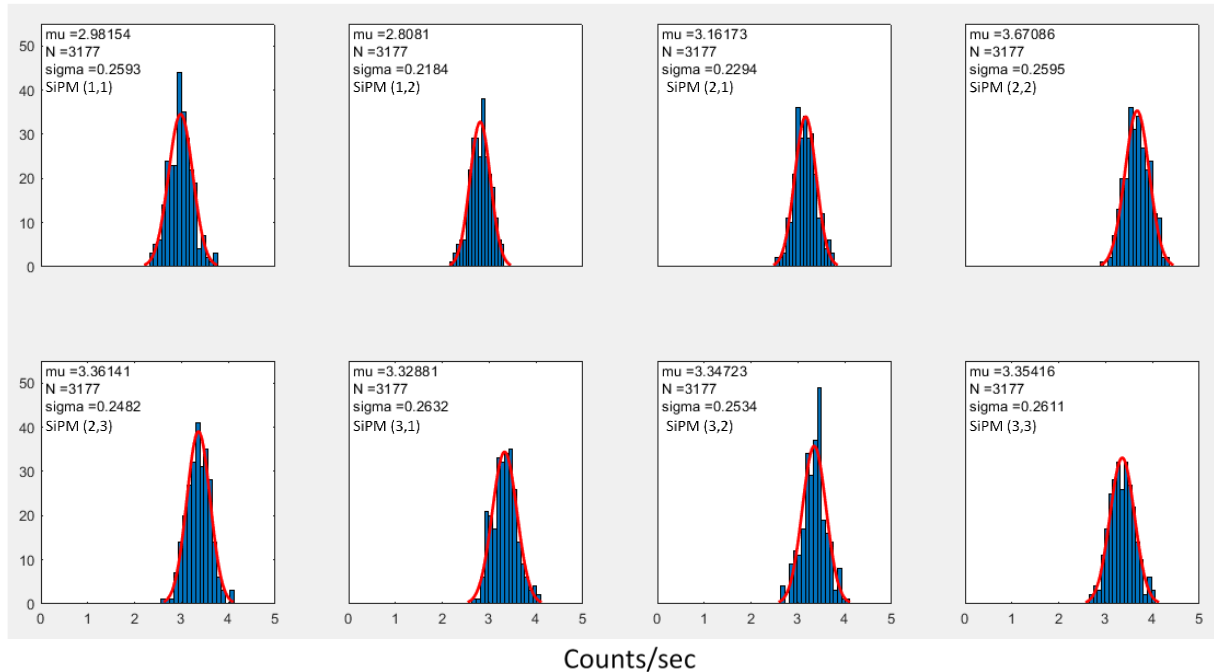


Figure 15: Plots of the distribution of the normalized SiPM count rates on Data Recorder 2 at ground level during the overnight run. The differences in N between figure 14 and figure 15 are due to Data Recorder 2 reading the count registers slightly slower than Data recorder 2.

The distributions show that the average count rate at ground level with no thunderstorm activity is around 3.5 counts/sec for each SiPM. To characterize the performance of the detector, it was also necessary to look at the distribution of counts per readout. A readout is when a Data Recorder reads all the count registers on the shield. When designing the payload, the team chose for the Data Recorders to read out the count registers as fast as possible instead of operating on an interrupt. The counts from the 1 MHz oscillator would then give microsecond timescale information for the read outs. Because of this, the time between each read out was not the same, so the counts per readout were normalized to a 1 millisecond time bin. This makes the figure below a distribution of the counts per millisecond for the detector during float. The readout periods with no change in counts were omitted to show more detail of the distribution.

$$\text{counts/ms} = (\text{SiPM counts since last read out}) / [10^3 / (1 \text{ Mhz counts since last readout})]$$

Figure 16 gives some of the most important information for SPACER from the HASP flight. Figure 16 gives an expected distribution for the detector behavior at ground levels and at background. This distribution gives a means of determining whether there is TGF activity in the area of the detector. A distribution at similar altitudes that is shifted to the right or with more of a tail may signal a detection of a TGF by SPACER.

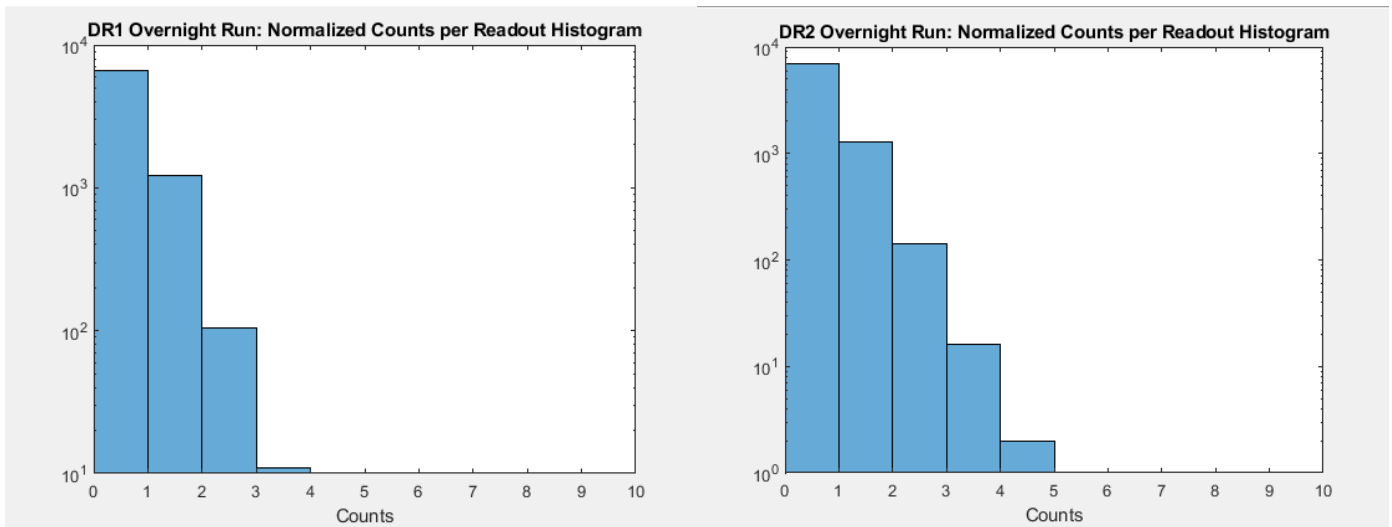


Figure 16: A semi-log distributions of the total number of SiPM counts per readout from the two Data Recorders at ground level. The number of counts per readout were normalized to a 1 millisecond time bin due to the time between readouts not being uniform.

12.2 Flight

For the flight all the SiPMs remained functional, but there were still some differences in efficiency as seen in 17 which is a plot of the SiPMs' total counts vs. time throughout the flight. The region where none of the SiPM record counts is due to HASP being powered down.

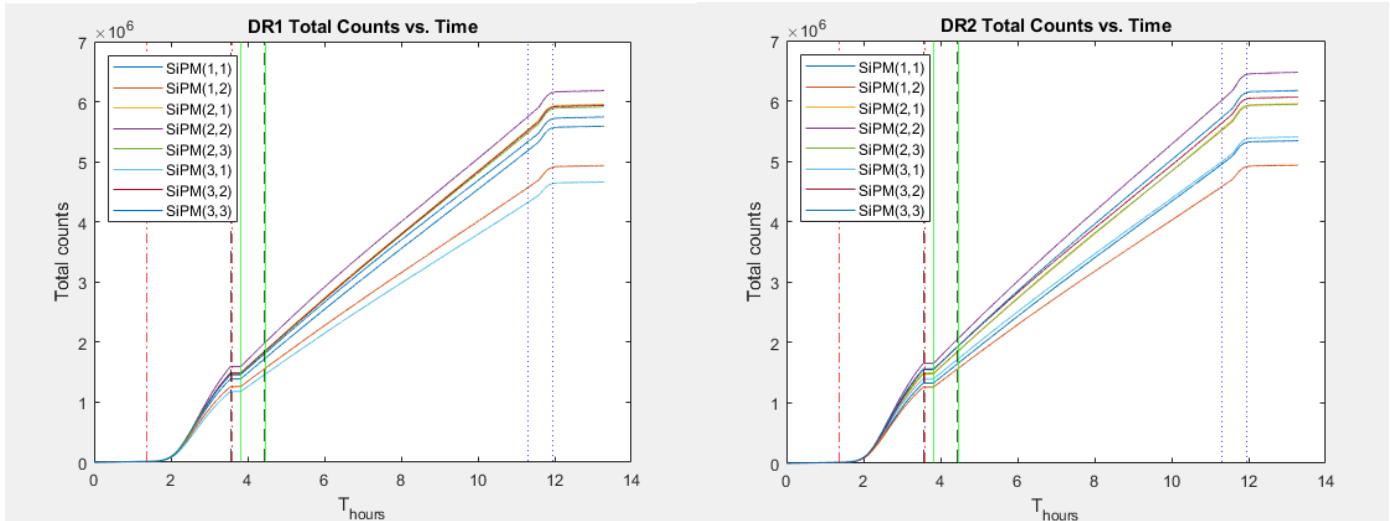


Figure 47: Plots of the SiPM's total counts vs. time for the duration of the flight with $T=0$ at 09/05/2019 11:40:00 UTC. With ascent (red-dashed line), descent (blue-dotted line), power downs (black dashed lines), and power ups (green dashed lines) marked.

Because of variations in efficiency across the SiPMs, the counts needed to be normalized to a single reference SiPM just as they had been for the overnight run. The same reference SiPM, SiPM (2,2) on Data Recorder 1, was chosen for the flight. The equation for the normalization is again shown below.

$$C_{\text{cor}} = C_{\text{meas}} * K_{\text{SiPM}}$$

$$K_{\text{SiPM}} = C_{\text{total(ref)}} / C_{\text{total}}$$

The total counts of the SiPMs with respect to time after the normalization can be seen in 18 below.

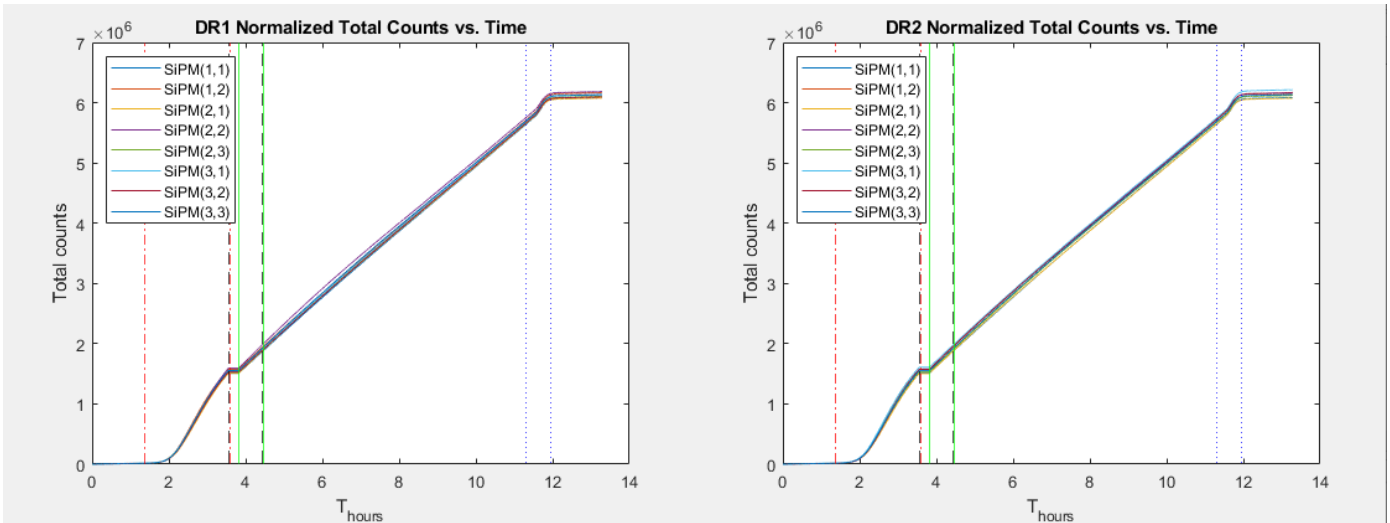


Figure 18: Plots of the SiPMs' normalized total counts vs. time for the duration of the flight with $T=0$ at 09/05/2019 11:40:00 UTC. With ascent (red-dashed line), descent (blue-dotted line), power downs (black dashed lines), and power ups (green dashed lines) marked.

The count rate of the SiPMs was also calculated, this was done by taking the change in normalized counts between successive readouts and dividing by the difference in times of the readouts. One-minute averages of the rate (counts/sec) were plotted as a function of altitude during ascent and are shown in 19.

$$\text{Rate} = [\text{Counts}(b) - \text{Counts}(a)] / [\text{Time}(b) - \text{Time}(a)]$$

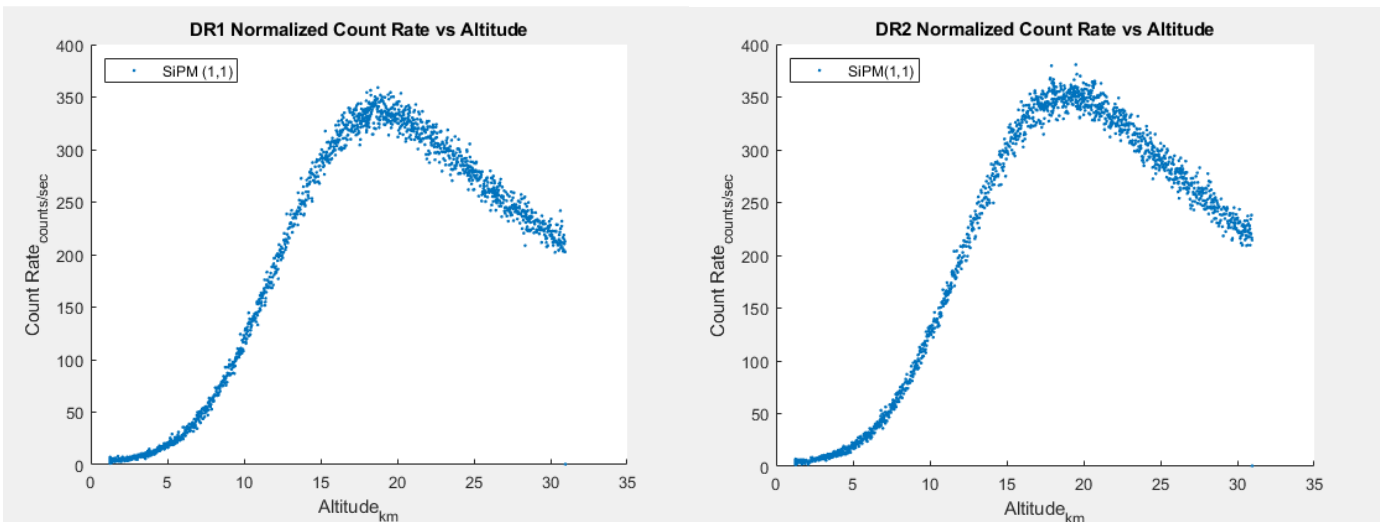


Figure 19: Plots of SiPM (1,1)'s normalized Count Rates vs. Altitude during ascent on Data Recorder 1 and 2.

In figure 19 the count rate of the SiPM on the two Data Recorders increases with altitude and passes through the well-known Pfozter maximum at approximately 18 km. To better

understand the performance of the detector at float, the count rates of the SiPMs needed to be analyzed as a function of time for the entire flight. A plot of the normalized SiPM count rates as a function of time for the flight is shown in figure 20.

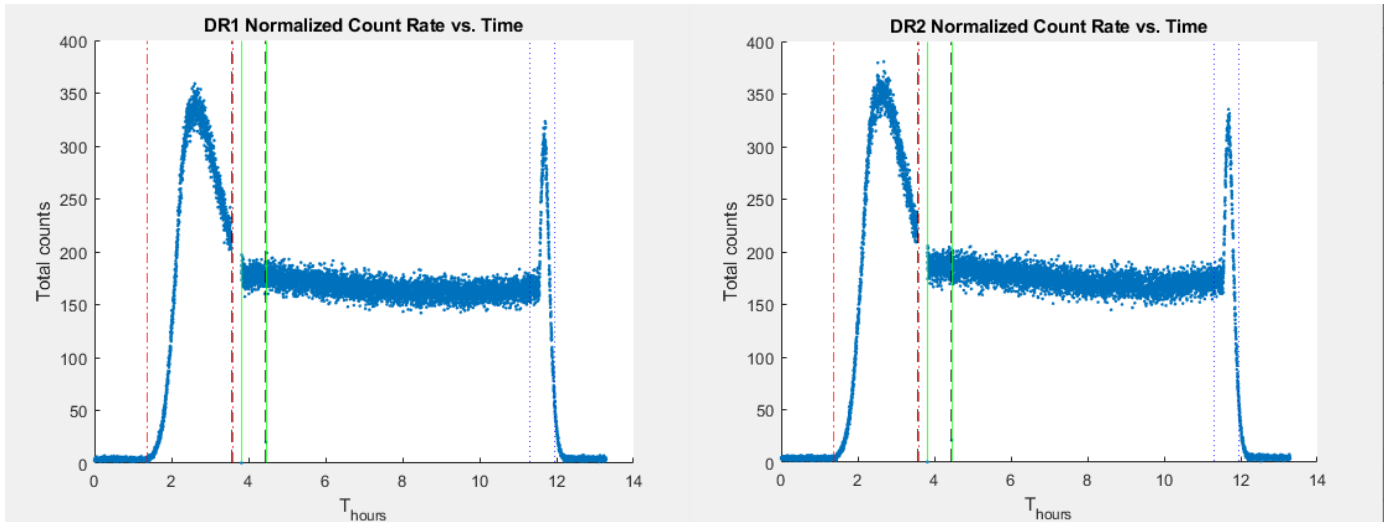
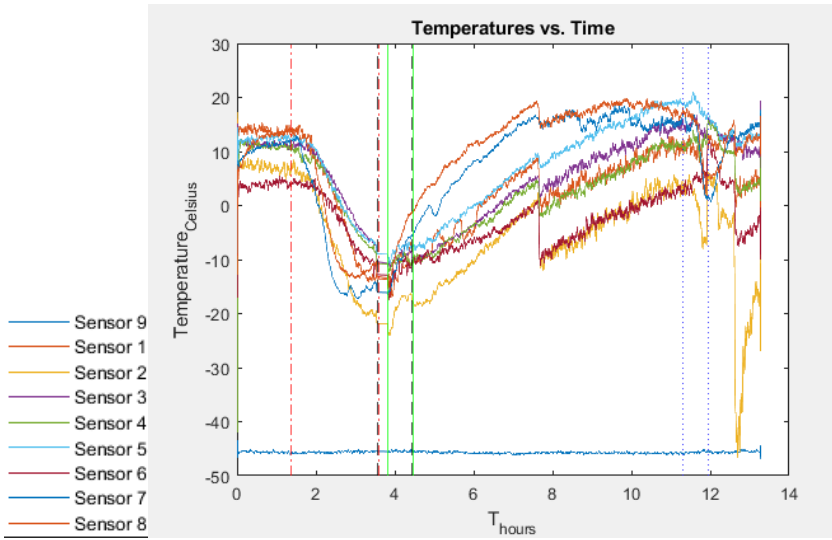


Figure 20: Plots of the SiPMs' normalized Count Rate vs. time for the duration of the flight with $T = 0$ at 09/05/2019 11:40:00 UTC. With ascent (red-dashed line), descent (blue-dotted line), power downs (black dashed lines), and power ups (green dashed lines) marked.

As the previous figure shows, the count rate of the SiPMs are decreasing even though the payload is remaining at the same altitude and experiencing a constant flux. This can be attributed to changes in the temperature of the payload, since the photon yield of the BGO crystals is inversely proportional to their temperature. As mentioned previously, the SPACER payload is fitted with nine temperature sensors to monitor the temperature of the crystals and critical electronics. Due to a limit on the analog inputs of an Arduino Due, some temperature sensors were given their own crystal while others were placed between two crystals. A plot of the temperature readings of the sensors plotted with respect to time is shown below.



Sensor #	Payload Location
1	Between Crystal (3,3) & (3,2)
2	Between Crystal (3,2) & (3,1)
3	Between Crystals (2,3) & (2,2)
4	Between Crystals (2,2) & (2,1)
5	Crystal (1,2)
6	Crystal (1,1)
7	Data Recorder 1
8	Data Recorder 2
9	12V DC/DC converter

Figure 21: Plots of the temperature readouts of all the temperature sensors vs. time for the duration of the flight with $T = 0$ at 09/05/2019 11:40:00 UTC. With ascent (red-dashed line), descent (blue-dotted line), power downs (black dashed lines), and power ups (green dashed lines) marked.

As shown above, sensor nine on the 12V DC/DC converter was outputting a voltage of zero volts and giving a temperature readout of $-47\text{ }^{\circ}\text{C}$ for the entire flight. There are also two discontinuous jumps in the readouts of all the temperature sensors just before hour eight and around hour 13. These discontinuities were cross checked with other events that took place during flight, but the team found no correlation. The temperature sensor with the smallest discontinuous jump was chosen as the temperature to be used for the payload. The temperature sensor with the smallest jump was sensor 5 on crystal (1,2). The count rate of the two SiPMs on crystal (1,2) are plotted along with the crystal's temperature as a function of time below.

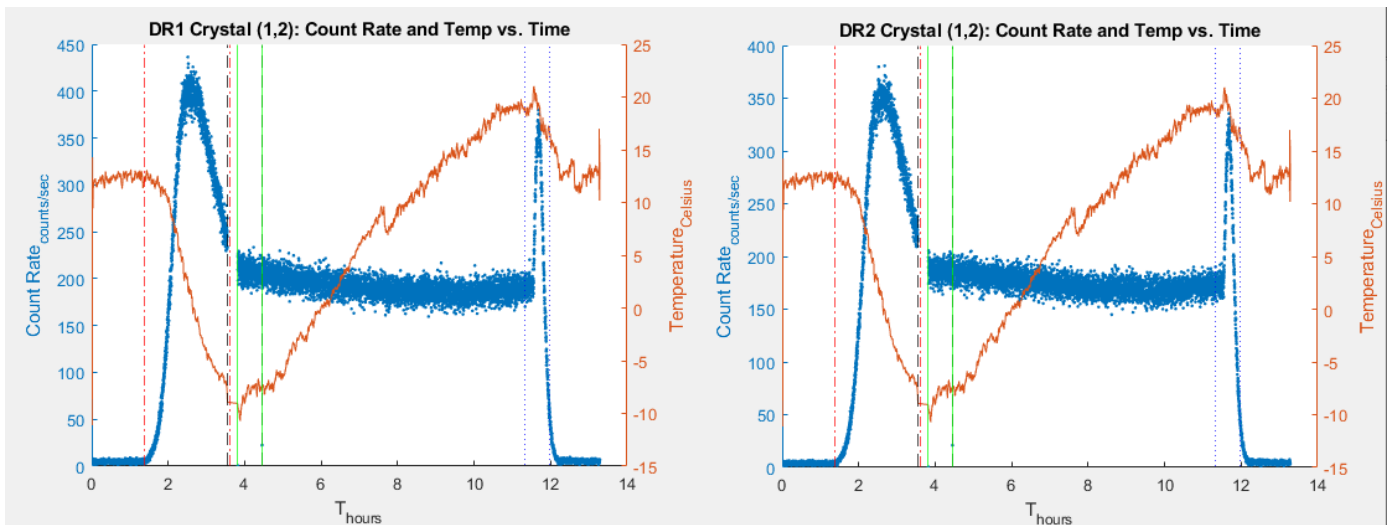


Figure 22: Plots of the temperature sensor on crystal (1,2) as well as the count rates of the two SiPMs on the crystal vs. time for the duration of the flight with $T = 0$ at 09/05/2019 11:40:00 UTC. With ascent (red-dashed line), descent (blue-dotted line), power downs (black dashed lines), and power ups

Figure 22 illustrates how the light yield of the BGO crystals, and in turn the count rate of the SiPMs, decrease as the temperature of the crystal increases. Because of this variation in detector performance, a correction for temperature needed to be applied to the float data. A time-dependent temperature correction for the float data was made by first selecting a reference period which would be the first hour of float. At each hour during float, the ratio of the average count rate during the first hour and the average count rate of the current hour was found. These ratios were then plotted as a function of time (hours at float), and a fit was applied to give the temperature correction. The time dependent temperature correction for SiPM (1,1) on Data Recorder 1 and how it was generated is shown below.

$$C_{cor} = C_{meas} * K_{crystal} * K_{temp}(t)$$

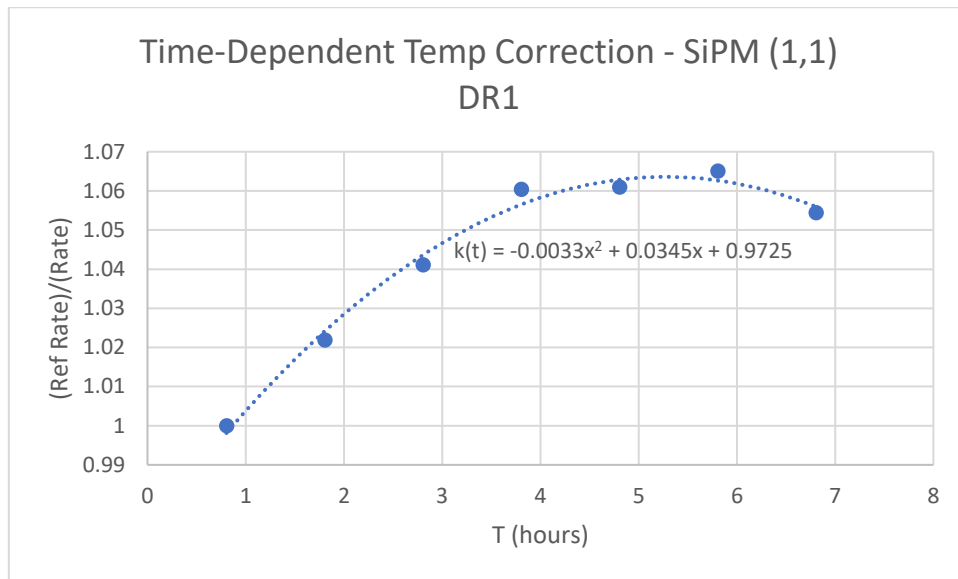


Figure 23: The ratios of the average count rate during hour one and the average count rates at different times during float plotted with respect to time and the fit given to the points that give the time dependent temperature correction $k(t)$ for SiPM (1,1) on Data Recorder 1.

For a full table of the temperature corrections for all the payload's SiPMs see Appendix L. Once this correction was applied, data was from different times at float could be compared with one another. Below are the Float count rates from the SiPMs on Data Recorder 1 before and after the corrections.

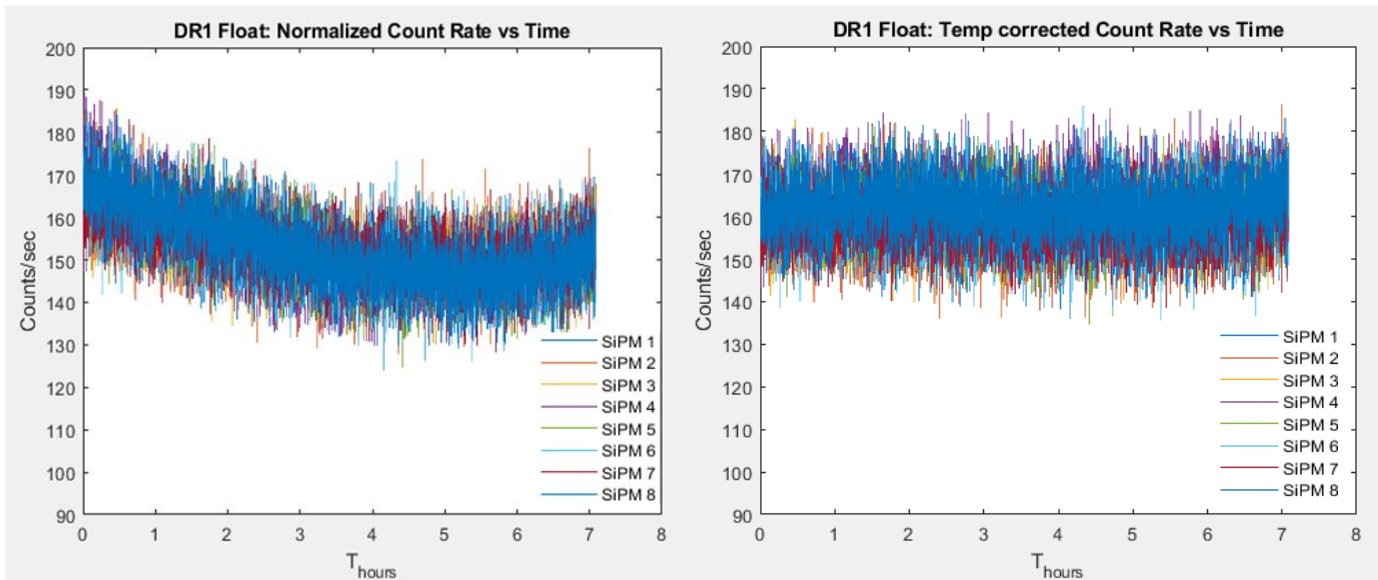


Figure 24: Plots of the SiPM count rates on Data Recorder 1 before and after the temperature correction was applied. $T = 0$ at 09/05/2019 16:12:08.

Once it was the counts had been normalized for differences in SiPM efficiency and temperature, the team was able to look at the distributions of the count rates for the different SiPMs at float. Below is the count rate (counts/sec) distribution of the SiPMs on Data Recorder 1 and 2 during Float.

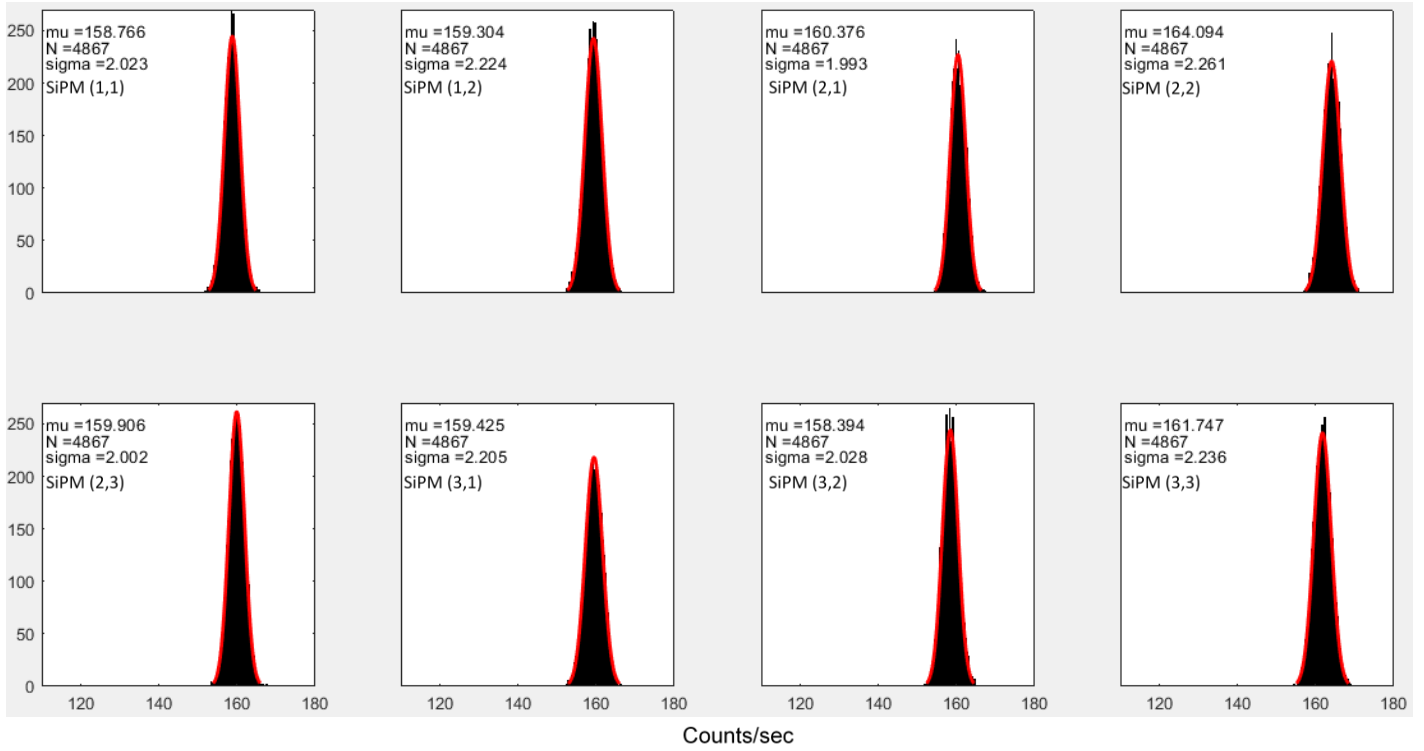


Figure 25: Plots of the distribution of the normalized SiPM count rates on Data Recorder 1 at float altitudes.

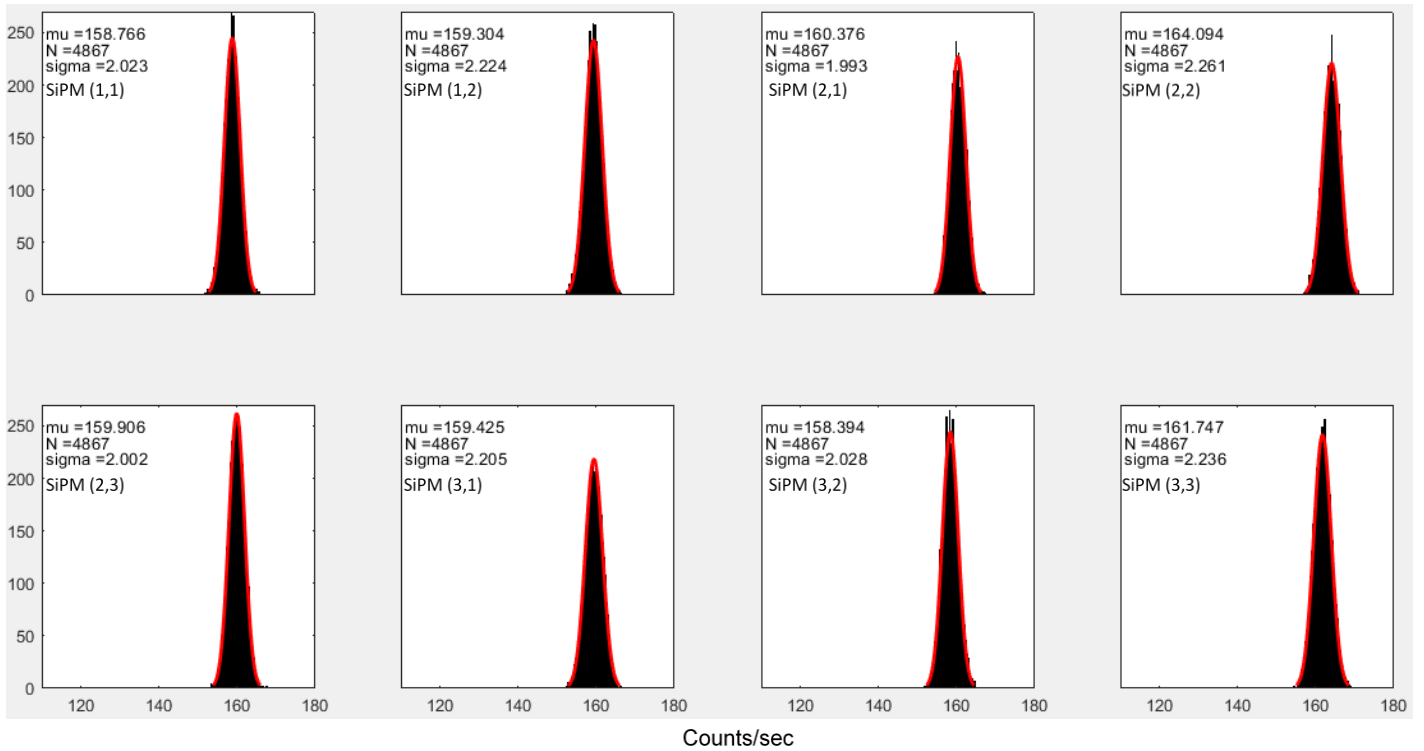


Figure 26: Plots of the distribution of the normalized SiPM count rates on Data Recorder 1 at float altitudes.

You can see that the distribution of normalized count rates for the SiPMs at float altitudes

range from 159 to 170 counts/sec, and these distributions are sharply peaked with no distribution having a sigma greater than 2.5. To characterize the performance of the detector, it was also necessary to look at the distribution of counts per readout. A readout is when a Data Recorder reads all the count registers on the shield. When designing the payload, the team chose for the Data Recorders to read out the count registers as fast as possible instead of operating on an interrupt. The counts from the 1 MHz oscillator would then give microsecond timescale information for the read outs. Because of this, the time between each read out was not the same, so the counts per readout were normalized to a 1 millisecond time bin. This makes the figure below a distribution of the counts per millisecond for the detector during float. The readout periods with no change in counts were omitted to show more detail of the distribution.

$$\text{counts/ms} = (\text{SiPM counts since last read out}) / [10^3 / (1 \text{ Mhz counts since last readout})]$$

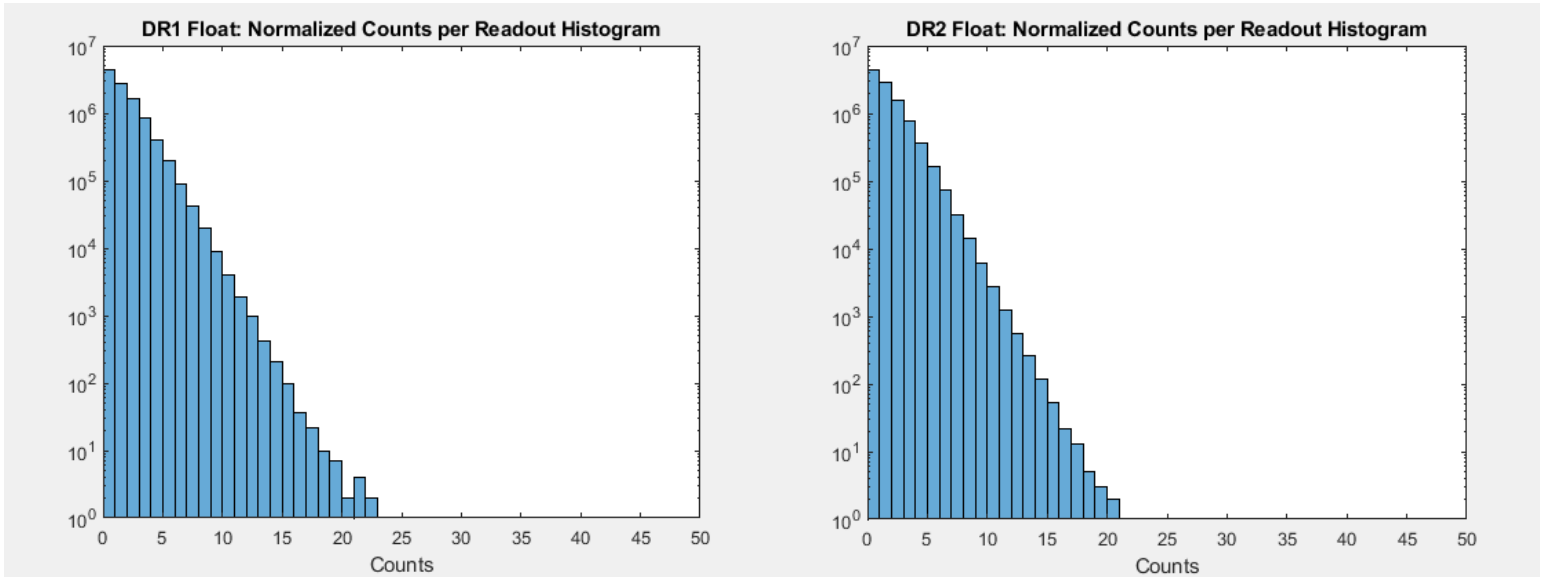


Figure 27: A semi-log distributions of the total number of SiPM counts per readout from the two Data Recorders at float altitudes. The number of counts per readout were normalized to a 1 millisecond time bin due to the time between readouts not being uniform.

Figure 27 gives some of the most important information for SPACER from the HASP flight. Figure 27 gives an expected distribution for the detector behavior at float altitudes establishes a baseline for detector performance. This distribution gives a means of determining whether there is TGF activity in the area of the detector. A distribution at similar altitudes that is shifted to the right or with more of a tail may signal a detection of a TGF by SPACER.

Simulations were then performed with EPICS 9.27 and Cosmos 8.035. Using the SPACER crystal configuration, particles were simulated from an isotropic half sphere. Muons were simulated with a spectral index of +4.7 and -2.7 for 1-10 GeV and 10-100 GeV, respectively [2 from Emmas poster]. Protons were thrown with a spectral index of -2.7 for 5 GeV (Fort Sumner's vertical cutoff rigidity) to 1 TeV, calculated using the geomagsphere.org's 2010

Internal Geomagnetic Field model IGRF and 2009 Tsyganenko External Geomagnetic Field model. After determining how many crystals were hit with each particle, the simulated hits were binned into millisecond time intervals based off the flux. 3 muons and 5 protons were equated to a millisecond time bin. The number of SiPM counts received during each readout was tallied and plotted in histograms (figures 28 & 29).

A minimum energy deposition threshold was applied to each crystal in simulations. In order to be detected by a crystal, a particle needed to deposit a minimum amount of energy into it. This threshold was determined by applying different thresholds to the muon simulations and comparing the resulting histogram to the bench test data. The threshold that matched the bench test data best was 5 MeV. This threshold gives a minimum sensitivity of the detector. takes into account the crystal attenuation and SiPM efficiencies. This threshold can be improved by covering the entire crystal face and using better quality BGOs.

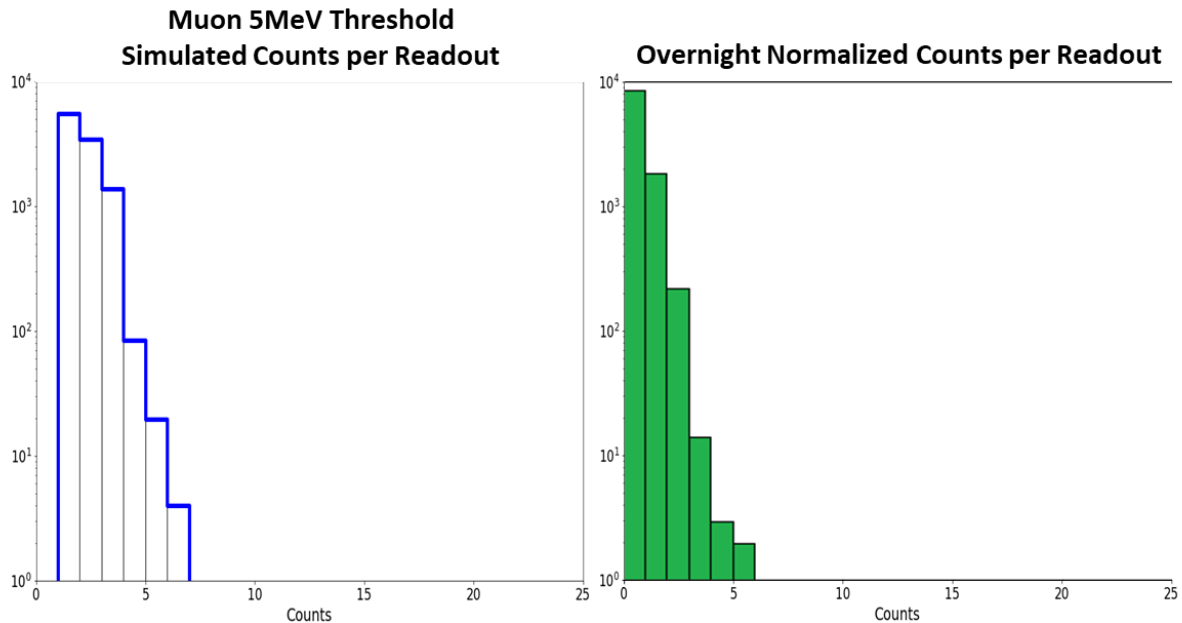


Figure 28: (Left) Simulated number of counts per readout during the bench test (three muons thrown at SPACER is a readout). A 5MeV threshold was applied to each crystal. This data has been scaled to the total number of counts in the bench test data. (Right) Bench test data showing the number of counts incremented during each readout. This data has temperature corrections and SiPM efficiencies applied.

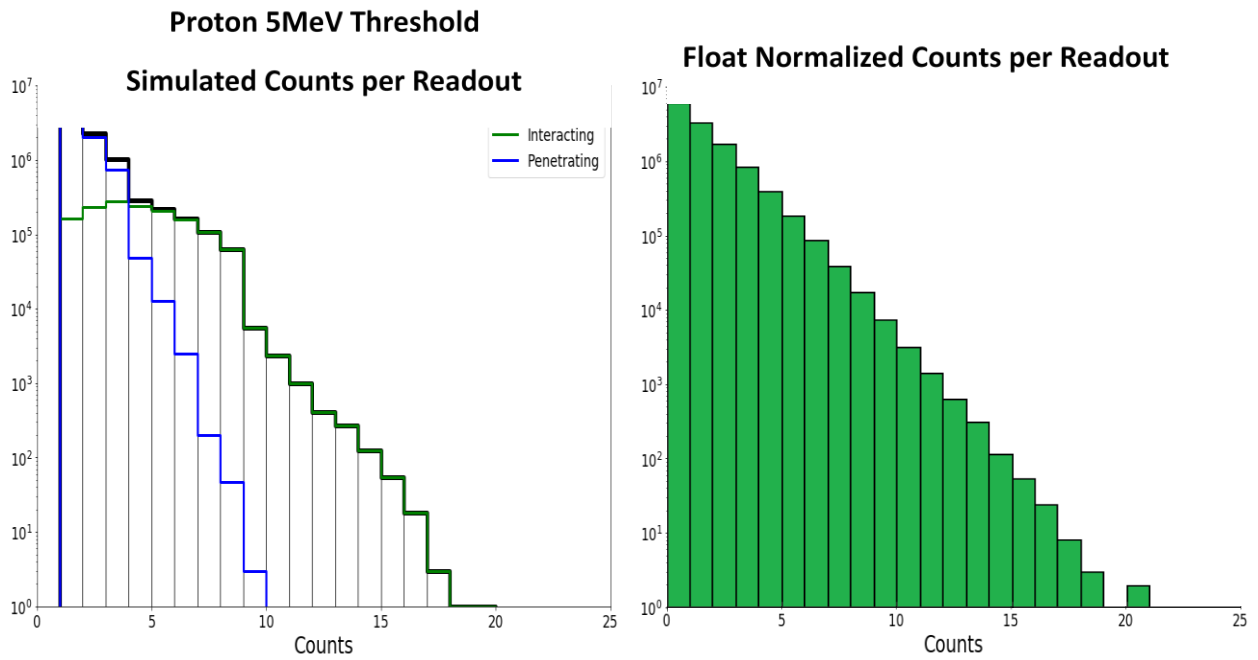


Figure 29: (Left) Simulated number of counts per readouts during float (five protons thrown at SPACER is a readout). A 5MeV threshold was applied to each crystal. This data has been scaled to the total number of counts in the float data. (Right) Float data showing the number of counts incremented during each readout. This data has temperature corrections and SiPM efficiencies applied.

13. Team Demographic

Name	Start Date	End Date	Role	Student Status	Race	Ethnicity	Gender	Disabled
Dana Browne	1/16/2019	Present	Faculty Advisor	Faculty	White		Male	No
Blaine Irle	1/16/2019	Present	Project Manager	Undergrad	White		Male	No
Josh Collins	1/16/2019	Present	Electrical	Staff	White		Male	No
Aaron Ryan	1/16/2019	Present	Electrical Lead	Graduate	White		Male	No
Robert Sac	1/16/2019	7/17/2019	Mechanical Lead	Undergrad	White		Male	No
Emma Western	1/16/2019	Present	Software Lead	Graduate	White		Female	No

14. Publications

Irle, Blaine. “Instrumentation Design of the Silicon Photomultiplier Array for Capturing Energetic Radiation (SPACER) Project.” Louisiana Space Council Meeting, 18 October 2019, LSU Student Union, Baton Rouge, LA. Poster Presentation.

Irle, Blaine. “Instrumentation Design of the Silicon Photomultiplier Array for Capturing Energetic Radiation (SPACER) Project.” American Geophysical Union Fall Meeting. 11 December 2019, Moscone Center, San Francisco, CA. Poster Presentation

Ryan, Aaron. “LaACES, USIP, HASP and Beyond: Development of the SPACER Gamma Detector.” Louisiana Space Council Meeting, 18 October 2019, LSU Student Union, Baton Rouge, LA.

Western, Emma. “Balloon flight results of Silicon Photomultiplier Array for Capturing Energetic Radiation (SPACER) Project” Louisiana Space Council Meeting, 18 October 2019, LSU Student Union, Baton Rouge, LA. Poster Presentation.

Western, Emma. “Balloon flight results of Silicon Photomultiplier Array for Capturing Energetic Radiation (SPACER) Project” American Geophysical Union Fall Meeting. 11 December 2019, Moscone Center, San Francisco, CA. Poster Presentation

15. References

- [1] J. R. Dwyer, D. M. Smith, S. A. Cummer, *Space Sci. Rev.* 173, 133-196 (2012)
- [2] G. J. Fishman, P. N. Bhat, R. Mallozzi, J. M. Horack, T. Koshut, C. Kouveliotou, G. N. Pendleton, C. A. Meegan, R. B. Wilson, W. S. Paciasas, S. J. Goodman, and H. J. Christian, *Science* 264, 1313 (1994). DOI: 10.1126/science.264.5163.1313.
- [3] Gaisser T.K., Stanev T., *Cosmic Rays*, <http://pdg.lbl.gov/2011/reviews/rpp2011-rev-cosmic-rays.pdf>, 2009
- [4] Alnussirat, Samer. “Observations of Energetic Emission From Thunderstorms: Terrestrial Gamma-ray Flashes and Gamma-ray Glows”, White Paper 2018
- [5] Wefel, John P., and T. Gregory Guzik. *Advanced Thin Ionization Calorimeter (ATIC) Balloon Experiment*. NASA, 2001, ntrs.nasa.gov/search.jsp?R=20010097885.

Appendix Table of Contents

Appendix A: PCB Designs	42
Appendix B: Schematics	43
Appendix C: Mechanical Drawings	46
Appendix D: SPACER Wiring Diagram	50
Appendix E: Calibration Data.....	51
Appendix F: Downlink Data Packet	52
Appendix G: Data Recorder Data Packet	56
Appendix H: Uplink Command Table	58
Appendix I: Test Flight Profile	60
Appendix J: Integration: Thermovac Test Timelines	61
Appendix K: HASP 2019 Flight Operation Timeline.....	62
Appendix L: SPACER Normalization Data	63

Appendix A – PCB Designs

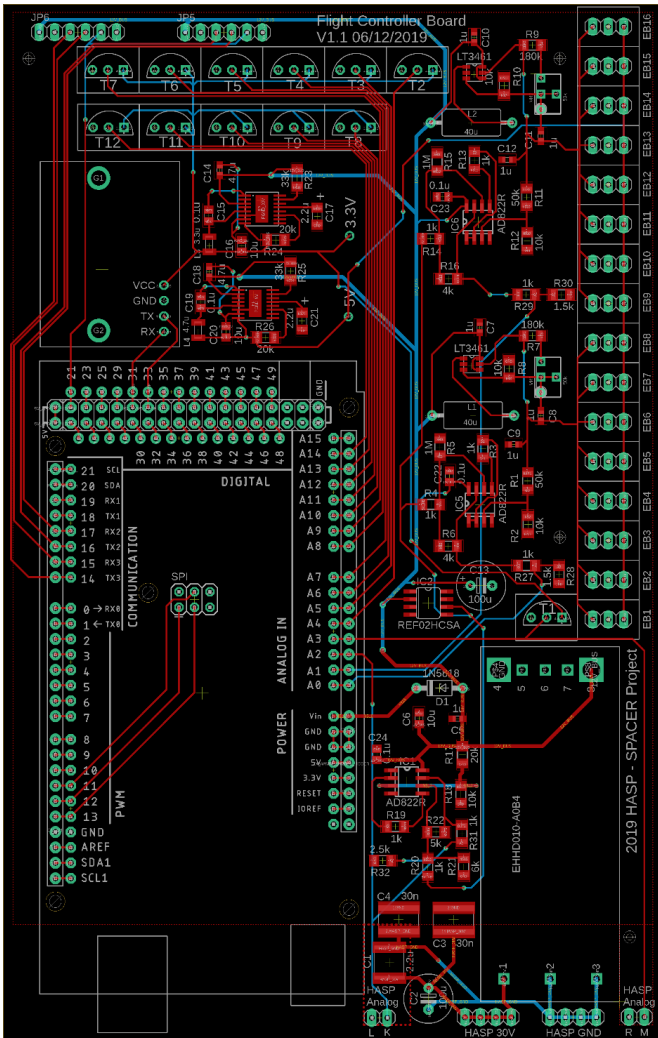


Figure 30: PCB design of the SPACER Flight Controller Shield

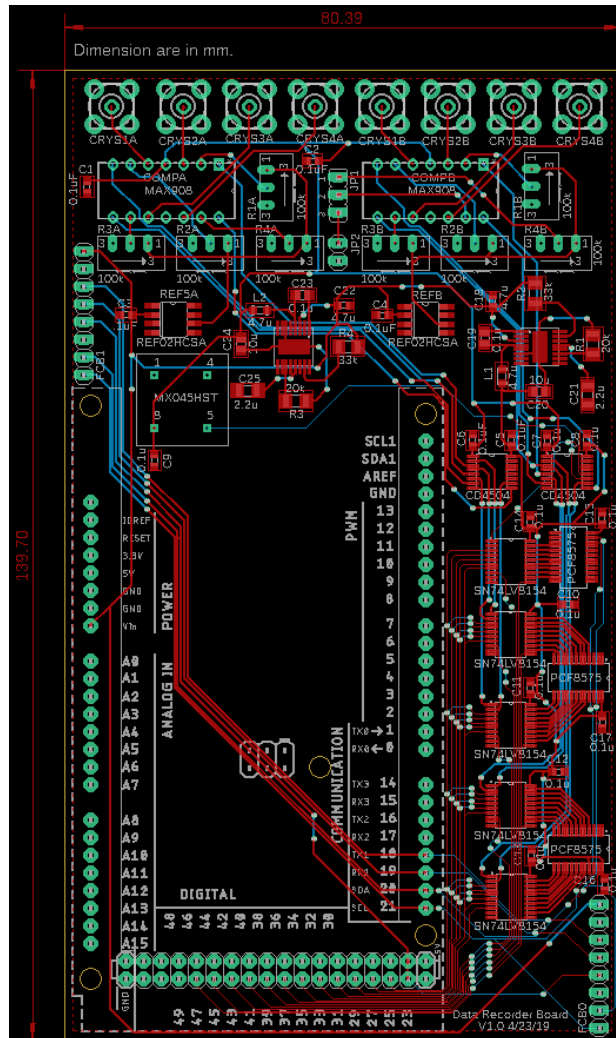


Figure 31: PCB design of the SPACER Data Recorder Shield

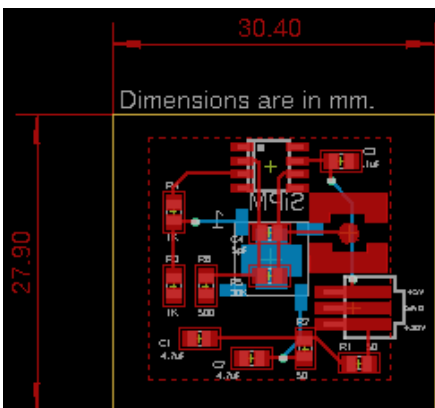


Figure 32: PCB design of the SPACER's SiPM endboards

Appendix B – Schematics

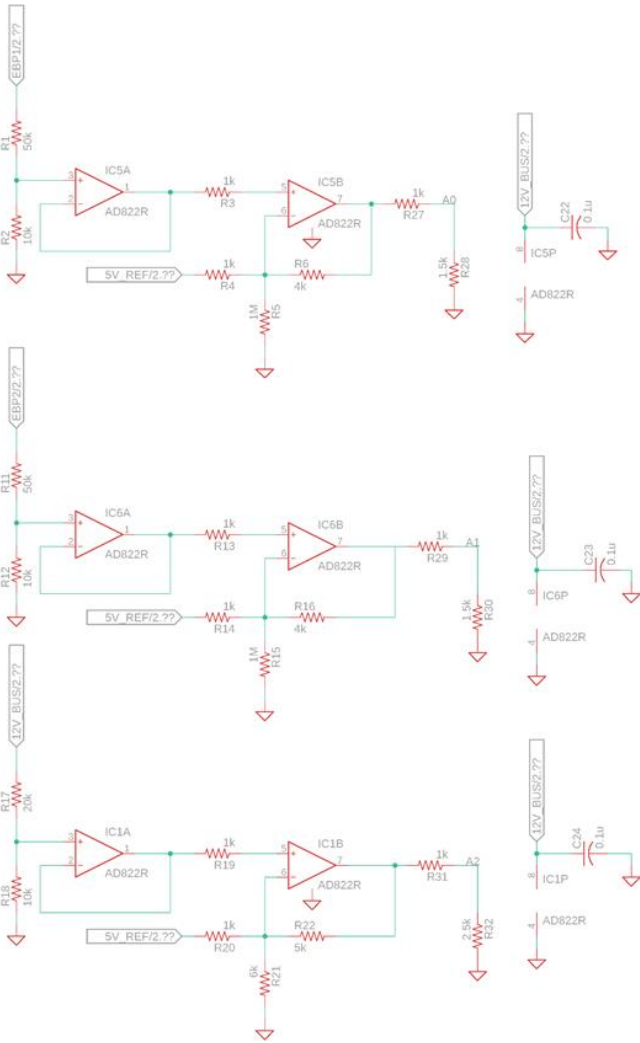


Figure 33: Schematic of SPACER's voltage monitoring circuits

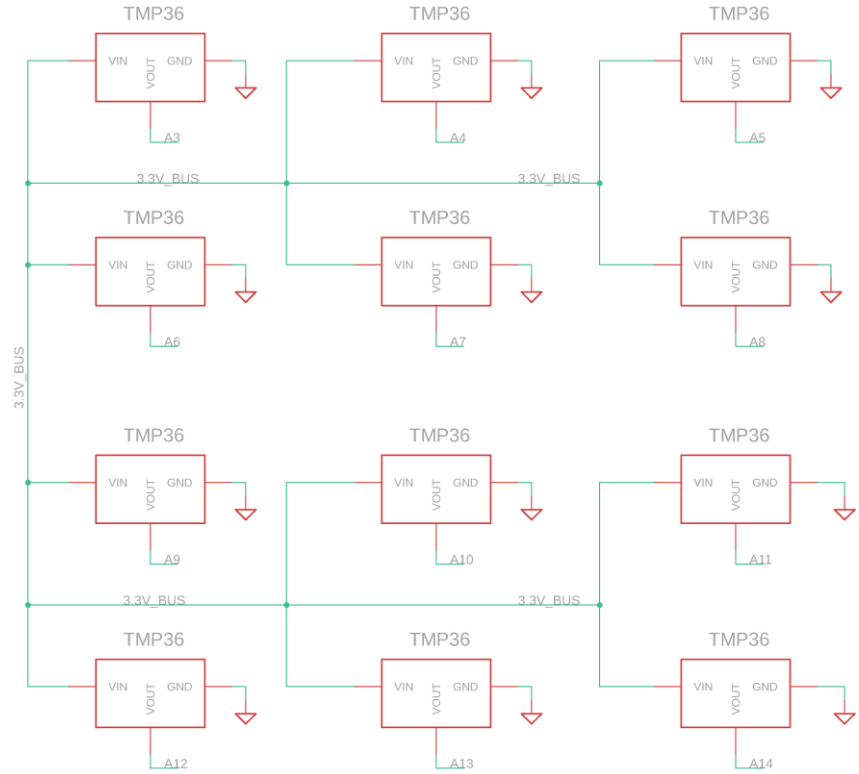


Figure 34: Schematic of SPACER's temperature monitoring circuits

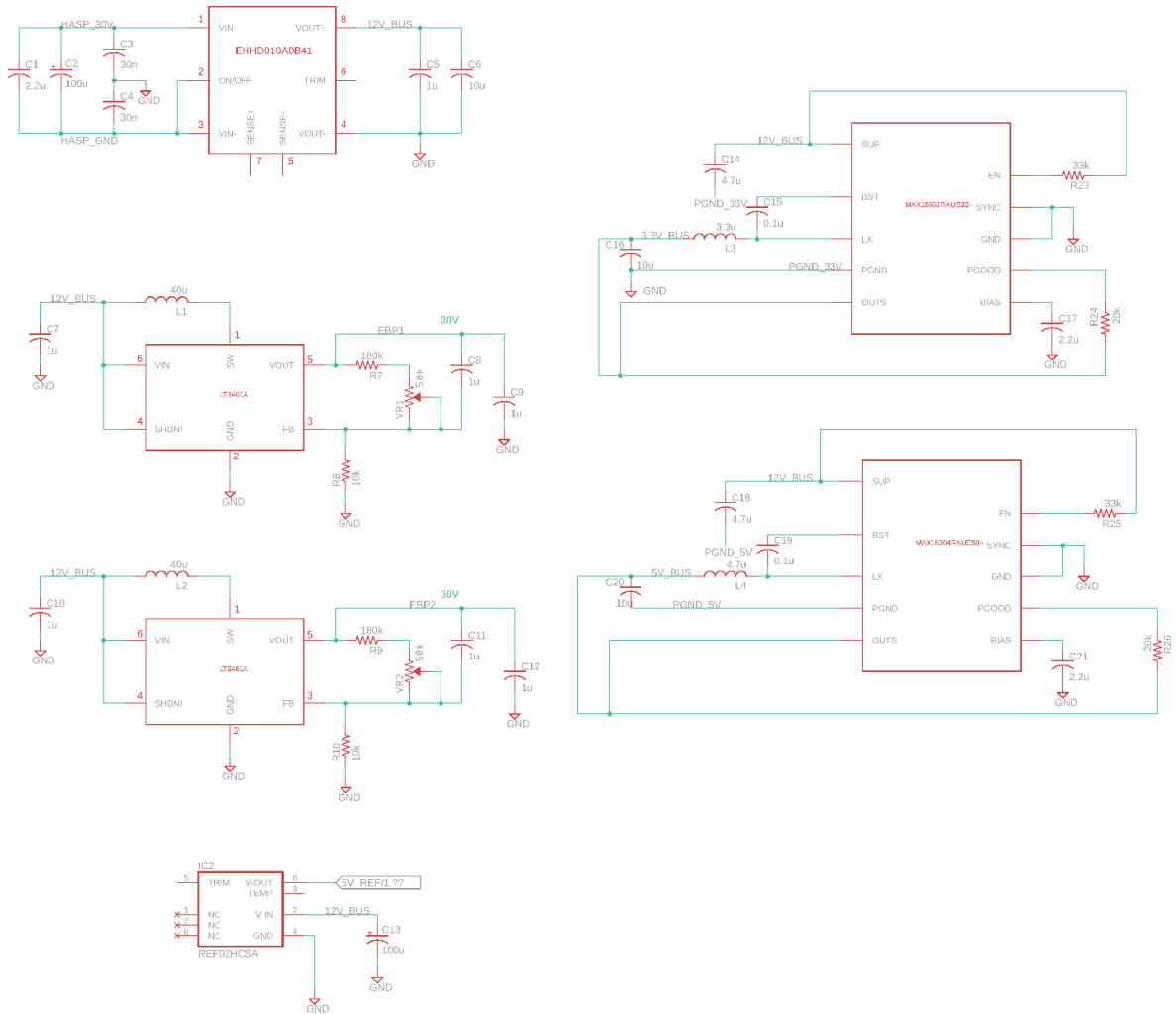


Figure 35: Schematic of the power regulation circuits on the SPACER Flight Controller shield

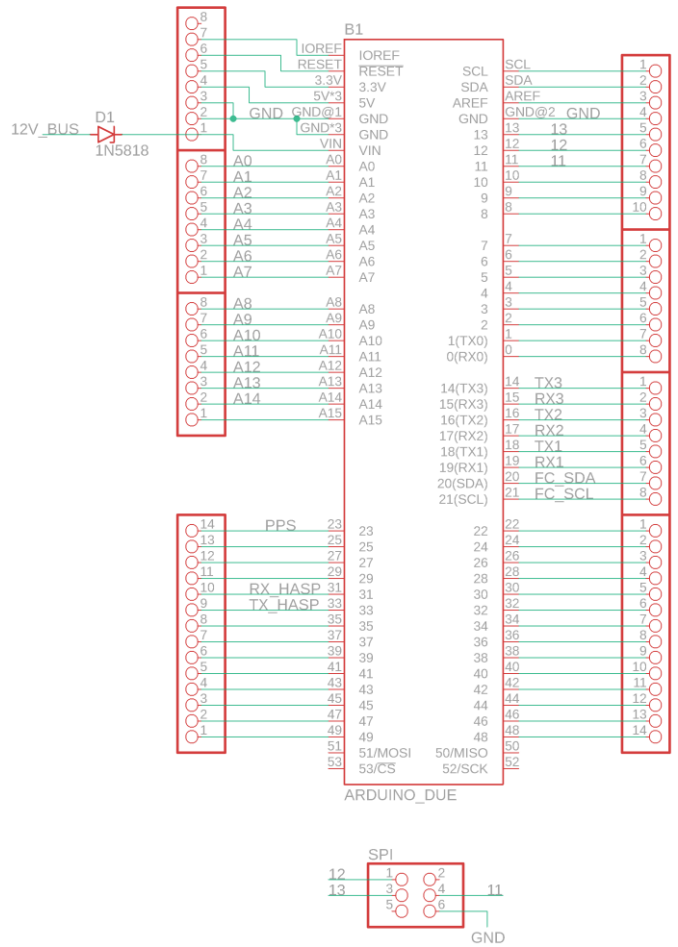
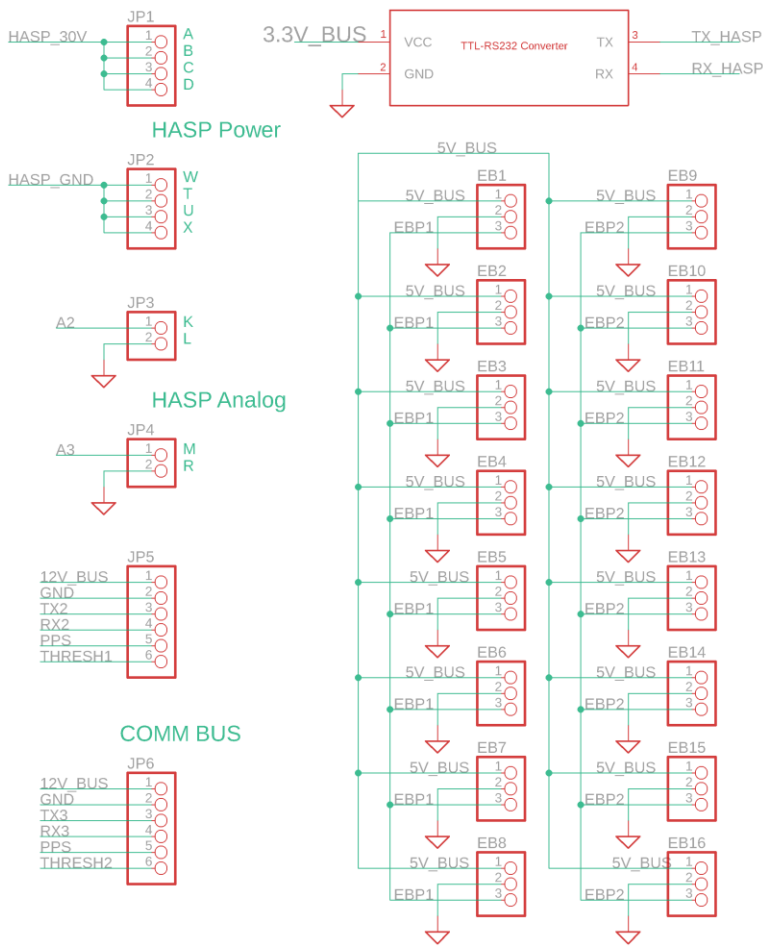


Figure 36: Different bus connections on the SPACER Flight Controller shield

Figure 37: Arduino Bus connections on the SPACER Flight Controller shield

Appendix C – Mechanical Drawings

ALL DIMENSIONS ARE IN INCHES

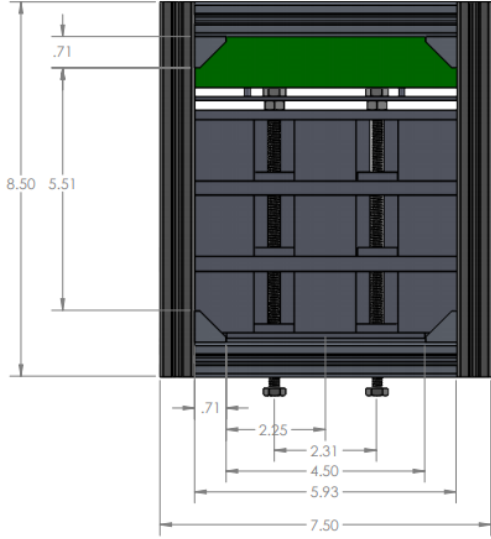


Figure 38: A front-view of the SPACER payload

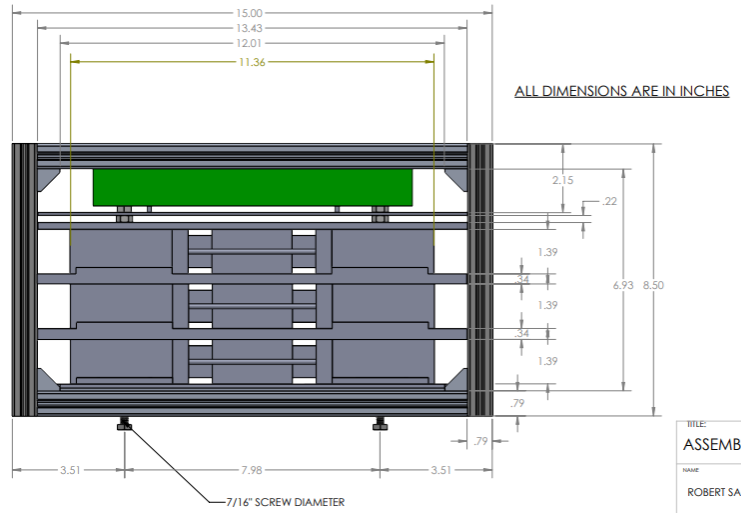


Figure 39: A front-view of the SPACER payload

TITLE:	
ASSEMBLY MODEL V1.1	
NAME:	DATE:
ROBERT SACK	APRIL 23, 2019

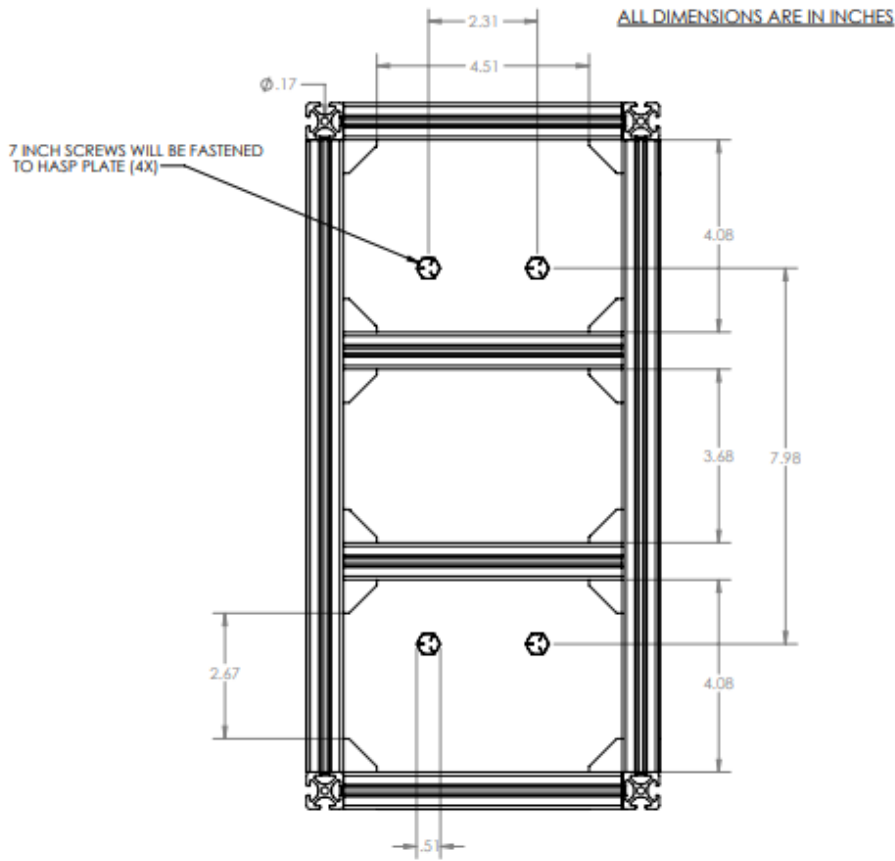


Figure 40: A bottom-view of the SPACER payload

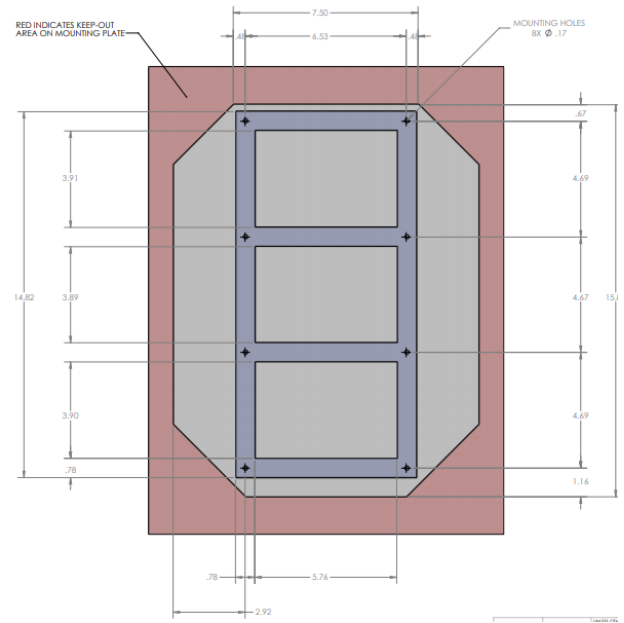


Figure 41: Mounting plan for SPACER

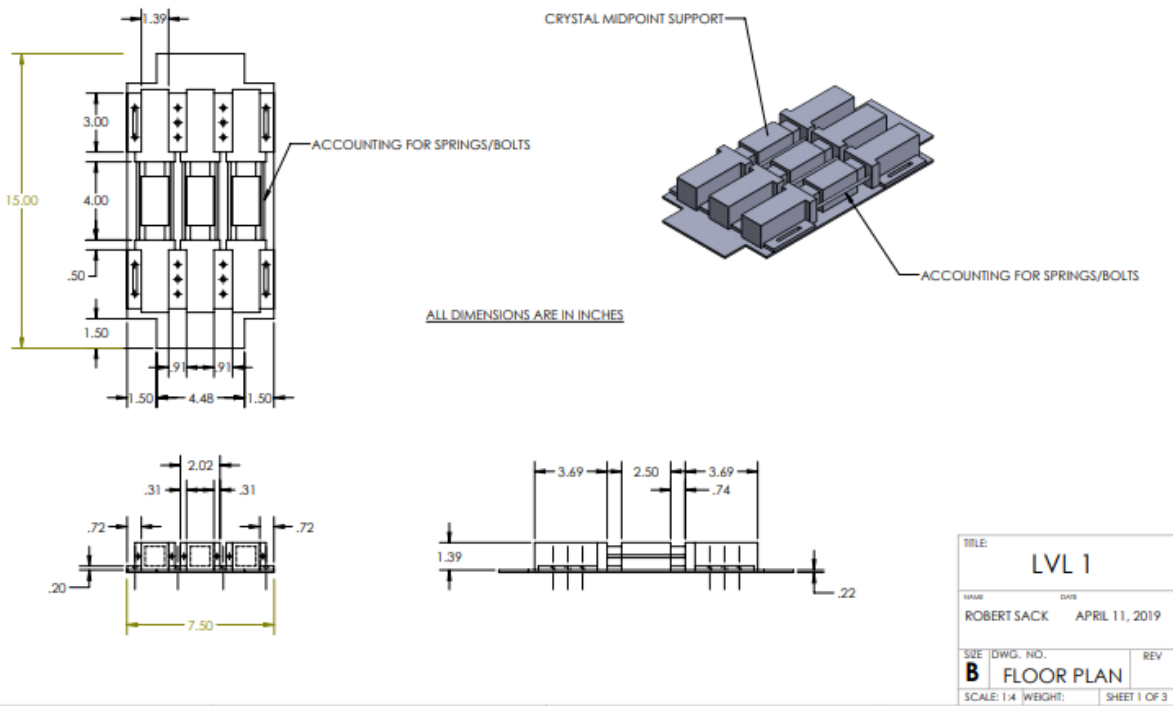


Figure 42: Mechanical Drawing of SPACER's 1st payload bay

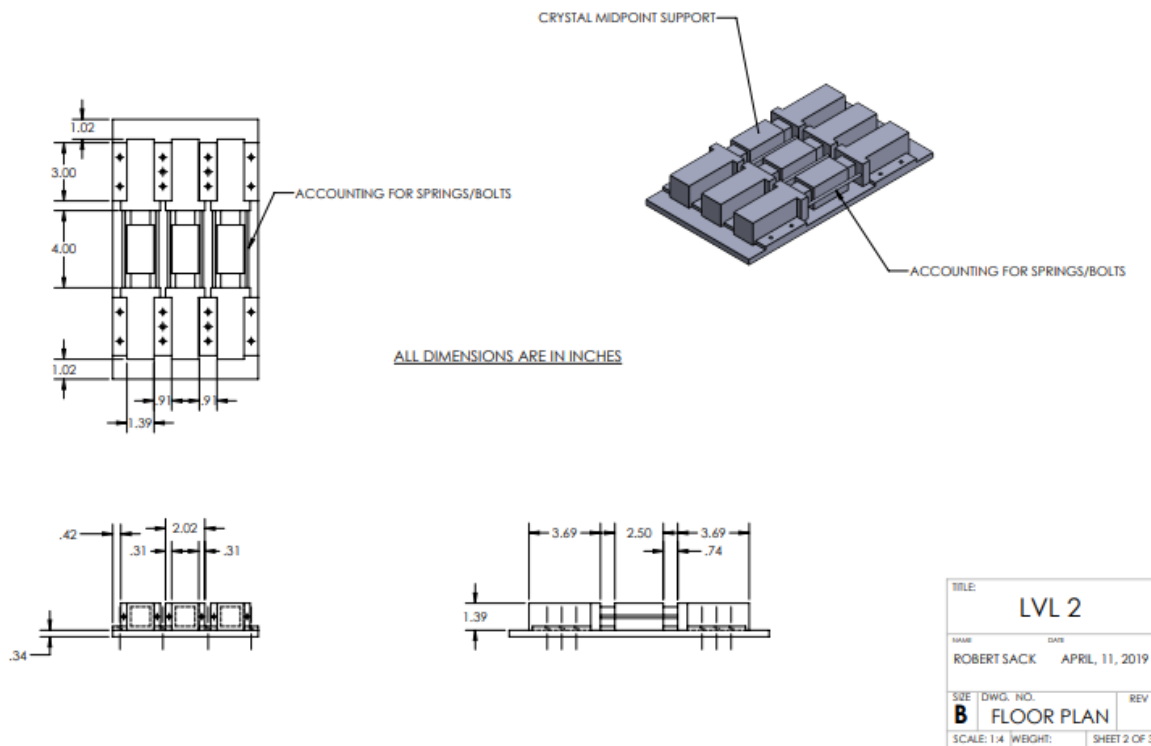


Figure 43: Mechanical Drawing of SPACER's 2nd payload bay

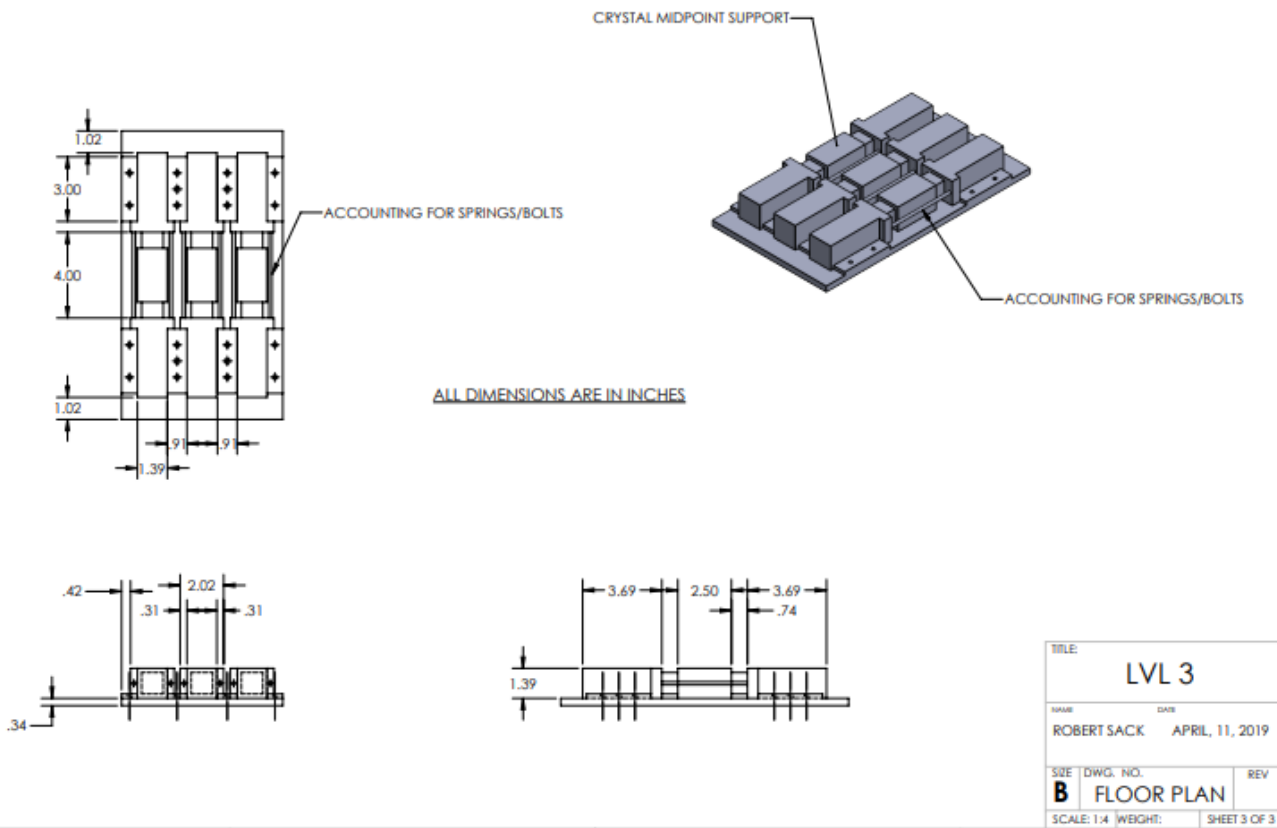


Figure 44: Mechanical Drawing of SPACER's 3rd payload bay

Appendix D – SPACER wiring Diagram

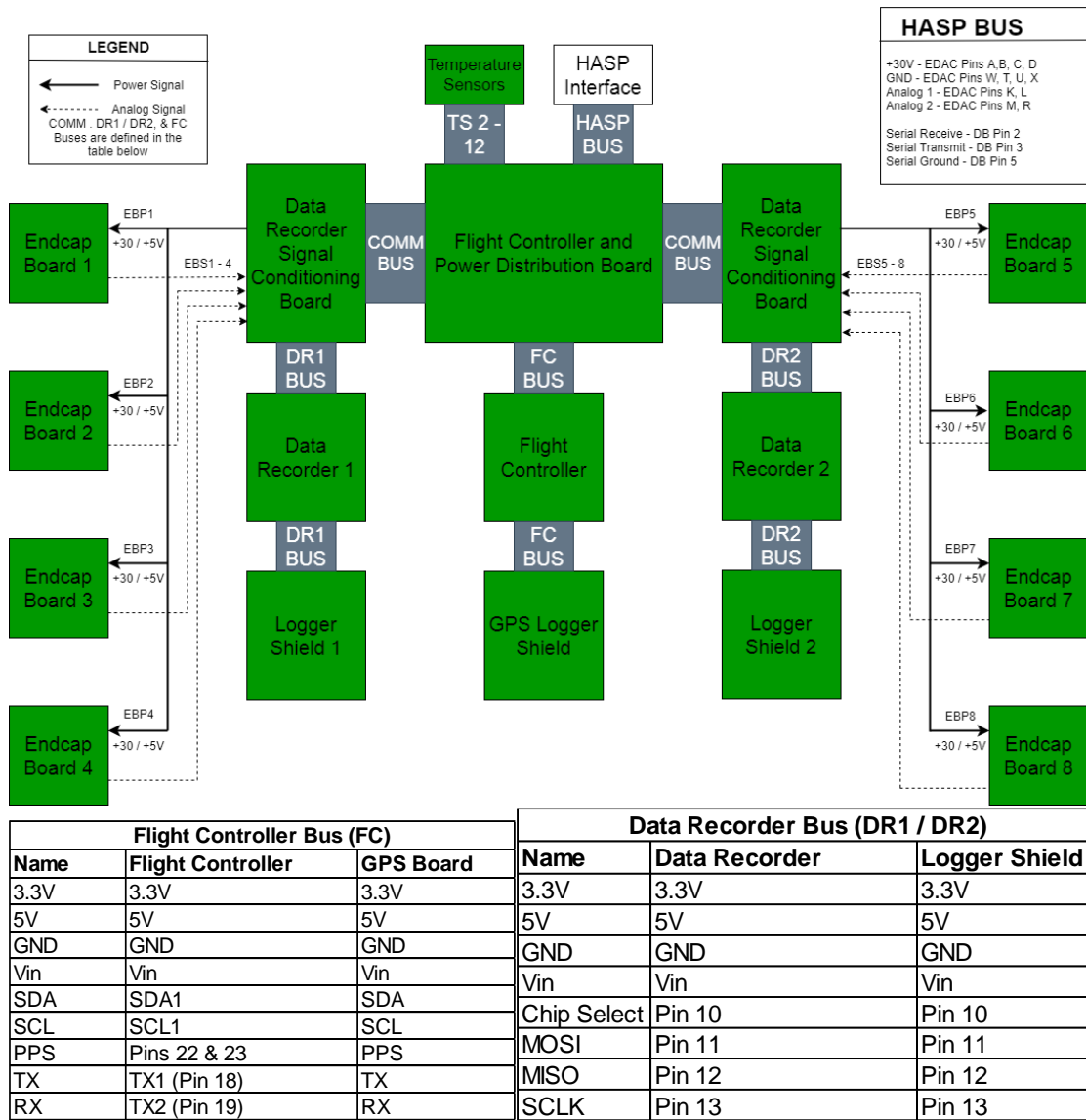


Figure 45: A SPACER wiring diagram and accompanying legend.

Appendix E – Calibration Data

Voltage	ADC (bank 1)	ADC (bank 2)
24	10.3438	23.7522
24.5	90.8759	105.9555
25	170.6709	185.8916
25.5	249.1946	264.8036
26	329.736	345.3521
26.5	407.4975	424.9821
27	486.9091	503.832
27.5	565.6935	584.4737
28	644.6087	663.4366
28.5	723.7504	742.6545
29	805.533	824.0502
29.5	882.4795	902.3045

Voltage	ADC Value
11.18	75.3611
11.47	226.2062
11.99	493.5028
12.46	734.5003
12.96	993.4382

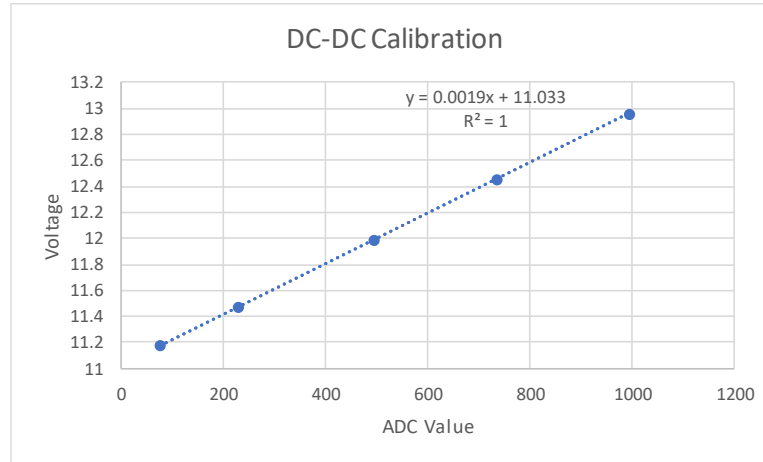


Figure 46: Voltage and ADC data used for the calibration of the voltage monitor circuits for the SiPM power banks (left) and the main DC-DC converter (right).

Figure 47: Calibration plots for the voltage monitor circuits for SPACER's main DC-DC converter.

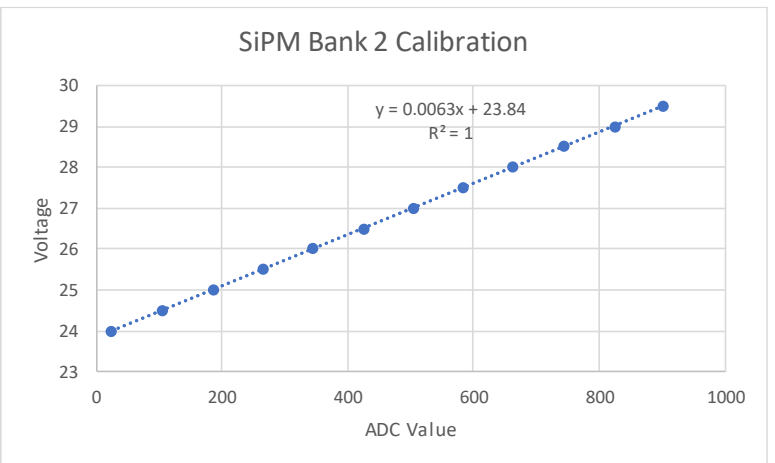
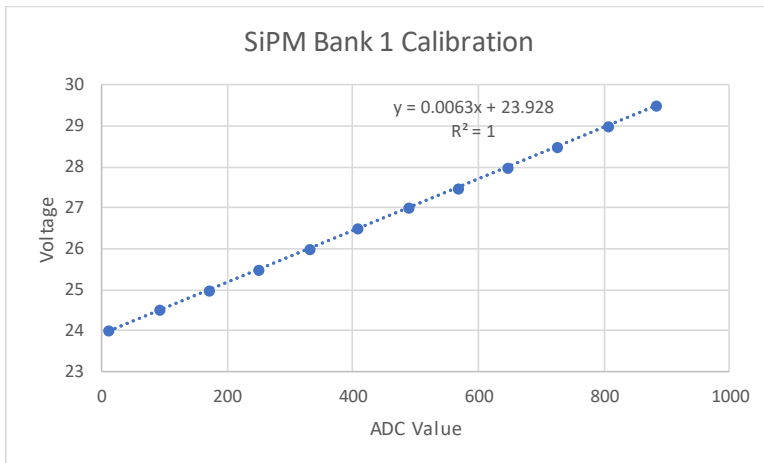


Figure 48: Calibration plots for the voltage monitor circuits for SPACER's two SiPM power banks.

Appendix F – Downlink Data Packet

Below is a table outlining all the components of the downlink data packet generated by SPACER’s Flight Controller as well as an example.

Downlink Data Transmission – readable ASCII format				
ASCII String Length	Starting Byte Number	Name – Excel Header	Description	Format
6 Bytes	0	Header	Record start indicator + “,”	START,
20 Bytes	6	Date and time stamp	The current year, month, day, hour, minute, second for the start of the data + “,”	MM/DD/YYYY HH:MM:SS,
11 Bytes	26	Altitude	Altitude from GPS	XXXXXXXXXX,
4 Bytes	37	# of Satellites	Number of satellites used by GPS for a fix	XXX,
4 Bytes	41	Fix Quality	Quality of the GPS fix	XXX,
11 Bytes	45	Uptime FC	Milliseconds Flight Computer has been on + “,”	XXXXXXXXXX,
4 Bytes	56	LC	Last Command (LC) received + “,” 0,0 = No command received X,X = Bytes from uplink command (see next section table)	X,X,
20 Bytes	60	LC Received Time	GPS timestamp LC was received + “,”	MM/DD/YYYY HH:MM:SS,
6 Bytes	80	SiPMV1	DR1 SiPM voltage + “,”	XX.XX,
6 Bytes	86	SiPMV2	DR2 SiPM voltage + “,”	XX.XX,

6 Bytes	92	DC/DC V	Output of main DC/DC converter + “,”	XX.XX,
6 Bytes	98	TMP1	Temperature for sensor 1 + “,” (in Kelvin)	XXX.X,
6 Bytes	104	TMP2	Temperature for sensor 2 + “,” (in Kelvin)	XXX.X,
6 Bytes	110	TMP3	Temperature for sensor 3 + “,” (in Kelvin)	XXX.X,
6 Bytes	116	TMP4	Temperature for sensor 4 + “,” (in Kelvin)	XXX.X,
6 Bytes	122	TMP5	Temperature for sensor 5 + “,” (in Kelvin)	XXX.X,
6 Bytes	128	TMP6	Temperature for sensor 6 + “,” (in Kelvin)	XXX.X,
6 Bytes	134	TMP7	Temperature for sensor 7 + “,” (in Kelvin)	XXX.X,
6 Bytes	140	TMP8	Temperature for sensor 8 + “,” (in Kelvin)	XXX.X,
6 Bytes	146	TMP9	Temperature for sensor 9 + “,” (in Kelvin)	XXX.X,
11 Bytes	152	Uptime DR1	Milliseconds DR1 has been on + “,”	XXXXXXXXXXXX,
11 Bytes	163	MHz1 Roll	Rollovers of DR1 MHz	XXXXXXXXXXXX,
11 Bytes	174	MHz1	Counts for DR1’s MHz Oscillator + “,”	XXXXXXXXXXXX,
11 Bytes	185	S1 C3A	DR1 SiPM counts + “,”	XXXXXXXXXXXX,
11 Bytes	196	S1 C2A	DR1 SiPM counts + “,”	XXXXXXXXXXXX,

11 Bytes	207	S1 C3B	DR1 SiPM counts + “,”	XXXXXXXXXXXX,
11 Bytes	218	S1 C2B	DR1 SiPM counts + “,”	XXXXXXXXXXXX,
11 Bytes	229	S1 C4A	DR1 SiPM counts + “,”	XXXXXXXXXXXX,
11 Bytes	240	S1 C1A	DR1 SiPM counts + “,”	XXXXXXXXXXXX,
11 Bytes	251	S1 C4B	DR1 SiPM counts + “,”	XXXXXXXXXXXX,
11 Bytes	262	S1 C1B	DR1 SiPM counts + “,”	XXXXXXXXXXXX,
2 Bytes	273	LC DR1	Last command received by DR1 + “,”	X,
2 Bytes	275	LC1 Result	Result of LC DR1 A = affirmative N = Negative 0 = No command received	X,
3 Bytes	277	TCV1	Voltage for DR1’s Test Crystal SiPMs + “,”	XX,
9 Bytes	280	Ignore DR1	Ignore status of DR1 SiPMs	XXXXXXXXXX,
6 Bytes	289	UID DR1	Last unique ID received by DR1	XXXXXX,
11 Bytes	295	Uptime DR2	Milliseconds DR2 has been on + “,”	XXXXXXXXXXXX,
11 Bytes	306	MHz2 Roll	Rollovers of DR2’s MHz	XXXXXXXXXXXX,
11 Bytes	317	MHz2	Counts for DR2’s MHz Oscillator + “,”	XXXXXXXXXXXX,
11 Bytes	328	S2 C3A	DR2 SiPM counts + “,”	XXXXXXXXXXXX,
11 Bytes	339	S2 C2A	DR2 SiPM counts + “,”	XXXXXXXXXXXX,
11 Bytes	350	S2 C3B	DR2 SiPM counts + “,”	XXXXXXXXXXXX,

11 Bytes	361	S2 C2B	DR2 SiPM counts + “;”	XXXXXXXXXXXX,
11 Bytes	372	S2 C4A	DR2 SiPM counts + “;”	XXXXXXXXXXXX,
11 Bytes	383	S2 C1A	DR2 SiPM counts + “;”	XXXXXXXXXXXX,
11 Bytes	394	S2 C4B	DR2 SiPM counts + “;”	XXXXXXXXXXXX,
11 Bytes	405	S2 C1B	DR2 SiPM counts + “;”	XXXXXXXXXXXX,
2 Bytes	416	LC DR2	Last command received by DR2 + “;”	X,
2 Bytes	418	LC2 Result	Result of LC DR2 A = affirmative N = Negative Z = No command received	X,
3 Bytes	420	TCV2	Voltage for DR2’s Test Crystal SiPMs + “;”	XX,
9 Bytes	423	Ignore DR2	Ignore status of DR2 SiPMs	XXXXXXXXXX,
6 Bytes	432	UID DR2	Last unique ID received by DR1	XXXXXX,
5 Bytes	438	Footer	Record end indicator + “;”	STOP;
2 Bytes	443	New Line		\n
Total bytes	445			

Example: START,07/14/2019

00:21:26,136.90,8,2,604845,0,0,N/A,27.48,27.50,12.08,16.40,25.91,28.16,25.57,25.87,22.96,21.50,20.74,25.07,604866,9196,35276,0,0,0,0,0,0,0,Z,Z,10,00000000,240,604915,9196,44123,0,0,0,0,0,0,Z,Z,10,00000000,241,STOP\n

Appendix G – Data Recorder Data Packet

Below is a table outlining all the components and an example of the format of the data packet generated by SPACER’s Data Recorder and saved to on-board memory.

Data Recorder Data Packet – readable ASCII format				
ASCII String Length	Starting Byte Number	Name – Excel Header	Description	Format
11 Bytes	0	Millis	Milliseconds Data Recorder has been on + “,”	XXXXXXXXXXXX,
1 Bytes	11	New second	New second call + “,”	X,
11 Bytes	12	MHz Rolls	Number of Rollovers of the MHz oscillator counter + “,”	XXXXXXXXXXXX,
11 Bytes	23	MHz	Number of counts on the MHz oscillator + “,”	XXXXXXXXXXXX,
11 Bytes	34	C3A	Number of counts on SiPM (1,1)	XXXXXXXXXXXX,
11 Bytes	45	C2A	Number of counts on SiPM (1,2)	XXXXXXXXXXXX,
11 Bytes	56	C3B	Number of counts on SiPM (2,1)	XXXXXXXXXXXX,
11 Bytes	67	C2B	Number of counts on SiPM (2,2)	XXXXXXXXXXXX,
11 Bytes	78	C4A	Number of counts on SiPM (2,3)	XXXXXXXXXXXX,
11 Bytes	89	C1A	Number of counts on SiPM (3,1)	XXXXXXXXXXXX,
11 Bytes	100	C4B	Number of counts on SiPM (3,2)	XXXXXXXXXXXX,

11 Bytes	111	C1B	Number of counts on SiPM (3,3)	XXXXXXXXXXXX,
----------	-----	-----	-----------------------------------	---------------

Logging in file 146DR.csv for code version DataRecorder_v7.0_190813

Millis	New Seco	MHz Rolls	MHz	C3A	C2A	C3B	C2B	C4A	C1A	C4B	C1B
1674775	1	25515	21101	53308	21548	9390	24786	4243	12410	2109	64082
1674776	1	25515	22280	53308	21548	9390	24786	4243	12410	2109	64082
1674778	1	25515	23462	53308	21548	9393	24787	4243	12410	2112	64084
1674779	1	25515	24674	53308	21549	9393	24787	4243	12410	2112	64084
1674780	1	25515	25913	53308	21549	9393	24787	4244	12411	2113	64085
1674781	1	25515	27162	53309	21549	9393	24788	4244	12411	2113	64086
1674783	1	25515	28418	53309	21549	9393	24788	4245	12411	2114	64087

Appendix H – Uplink Command Table

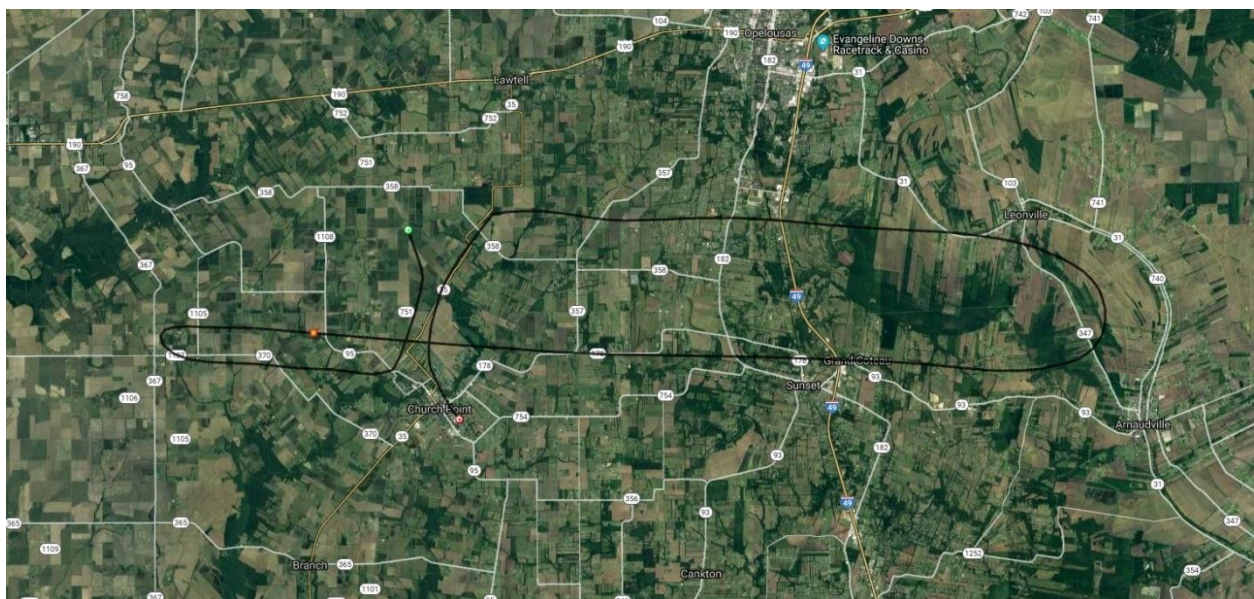
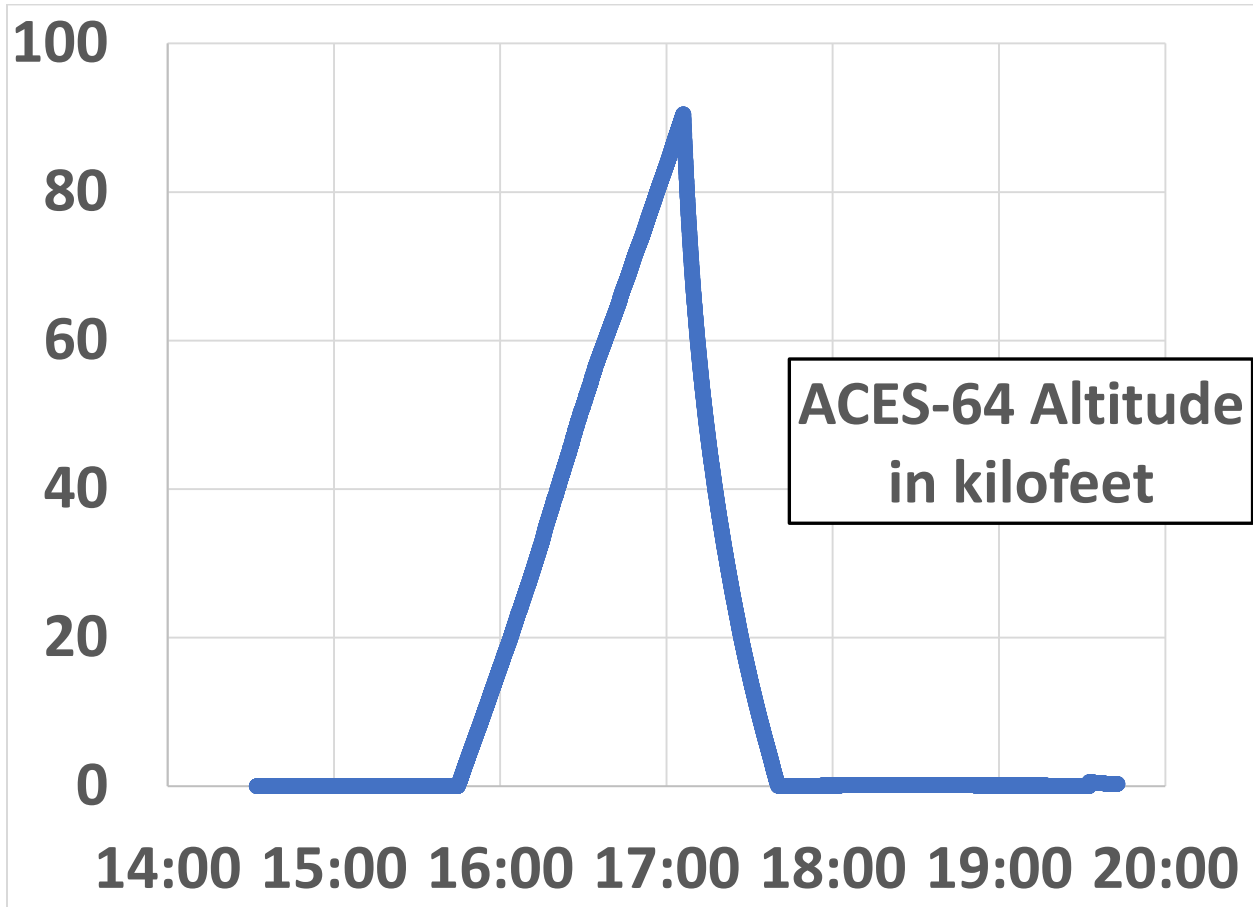
Below is a table of all of SPACER’s uplink commands and the action they cause.

Byte 1 (Hexadecimal)	Byte 2 (Hexadecimal)	Command
0x01	0x01	Ignore SiPM 1 for Data Recorder (DR) 1
0x01	0x02	Ignore SiPM 2 for DR 1
0x01	0x03	Ignore SiPM 3 for DR 1
0x01	0x04	Ignore SiPM 4 for DR 1
0x01	0x05	Ignore SiPM 5 for DR 1
0x01	0x06	Ignore SiPM 6 for DR 1
0x01	0x07	Ignore SiPM 7 for DR 1
0x01	0x08	Ignore SiPM 8 for DR 1
0x01	0x09	Set bias voltage DR 1’s Test Crystal to default value
0x01	0x0A	Increase bias voltage DR 1’s Test Crystal
0x01	0x0B	Decrease bias voltage DR 1’s Test Crystal
0x02	0x01	Ignore SiPM 1 for DR 2
0x02	0x02	Ignore SiPM 2 for DR 2
0x02	0x03	Ignore SiPM 3 for DR 2
0x02	0x04	Ignore SiPM 4 for DR 2
0x02	0x05	Ignore SiPM 5 for DR 2
0x02	0x06	Ignore SiPM 6 for DR 2
0x02	0x07	Ignore SiPM 7 for DR 2

0x02	0x08	Ignore SiPM 8 for DR 2
0x02	0x09	Set bias voltage DR 2's Test Crystal to default value
0x02	0x0A	Increase bias voltage DR 2's Test Crystal
0x02	0x0B	Decrease bias voltage DR 2's Test Crystal

Appendix I – Test Flight Profile

Below is the altitude file of the test flight plotted as a function of UTC time on June 6th, 2019 as well as the flight path of payload.



Appendix J – HASP Integration: Thermovac Test Timelines

1st ThermoVac Test		
Date	Time (UTC)	Action
7/17/2019	13:57:00	Door Close
7/17/2019	14:35:00	Command 0x01 0x01 requested
7/17/2019	15:02:00	Command 0x01 0x01 faulty execution
7/17/2019	15:02:00	Command 0x02 0x01 requested
7/17/2019	15:11:00	Command 0x02 0x01 faulty execution
7/17/2019	15:15:00	Command 0x01 0x01 requested
7/17/2019	15:24:00	Command 0x01 0x01 faulty execution
7/17/2019	15:26:00	Command 0x01 0x02 requested
7/17/2019	15:44:00	Command 0x01 0x02 executed
7/17/2019	15:45:00	SiPMs stop counting
7/17/2019	15:46:00	Power Cycle requested
7/17/2019	15:49:00	Power Cycle executed
7/17/2019	15:55:00	Command 0x02 0x0A requested
7/17/2019	16:04:00	Command 0x02 0x0A executed
7/17/2019	16:04:00	Command 0x01 0x0B requested
7/17/2019	16:12:00	Command 0x01 0x0B executed
7/17/2019	16:17:00	Command 0x01 0x03 requested
7/17/2019	16:22:00	Command 0x01 0x03 executed
7/17/2019	16:23:00	Command 0x02 0x03 requested
7/18/2019	16:34:00	Command 0x02 0x03 executed
7/19/2019	16:48:00	Command 0x02 0x09 requested
7/20/2019	16:53:00	Command 0x02 0x09 partial execution
7/21/2019	16:53:00	Command 0x01 0x09 requested
7/22/2019	16:54:00	Command 0x01 0x09 partial execution
7/23/2019	17:20:00	Command 0x02 0x04 requested
7/24/2019	17:25:00	Command 0x02 0x04 executed
7/25/2019	19:12:00	Command 0x01 0x05 requested
7/26/2019	19:28:00	Command 0x01 0x05 executed
7/27/2019	19:30:00	End test

Figure 46: Timeline of events for the first thermovac test

2nd ThermoVac Test		
Date	Time (UTC)	Action
7/18/2019	14:04:00	Door Close
7/18/2019	14:04:00	Fix Obtained
7/18/2019	14:16:00	Command 0x01 0x01 requested
7/18/2019	14:17:00	Command 0x01 0x01 executed
7/18/2019	14:23:00	Command 0x01 0x02 requested
7/18/2019	14:24:00	Command 0x01 0x02 executed
7/18/2019	14:37:00	SiPMs stop counting
7/18/2019	14:48:00	Power Cycle requested
7/18/2019	14:48:00	Power cycled executed
7/18/2019	14:49:00	Data Recorders unresponsive
7/18/2019	14:59:00	Power Cycle requested
7/18/2019	15:00:00	Power Cycle executed
7/18/2019	15:01:00	Data Recorders unresponsive
7/18/2019	16:30:00	Power Cycle Reuested
7/18/2019	16:33:00	Power down
7/18/2019	16:42:00	Power up
7/18/2019	16:43:00	Data Recorders unresponsive
7/18/2019	20:00:00	End test

Figure 47: Timeline of events for the second thermovac test

Appendix K – HASP 2019 Flight Operations Timeline

UTC Time	Event	T
08/28/2019 15:00:00	Arrive at Hangar	-07:20:40:00
08/28/2019 16:30:00	Attached to HASP gondola	-07:19:10:00
08/28/2019 16:33:34	Power up	-07:19:06:26
08/28/2019 16:35:00	Command 0x01 0x01 requested	-07:19:05:00
08/28/2019 16:35:49	Command 0x01 0x01 confirmed	-07:19:04:11
08/28/2019 16:36:00	Command 0x02 0x01 requested	-07:19:04:00
08/28/2019 16:36:29	Command 0x02 0x01 confirmed	-07:19:03:31
08/28/2019 16:37:14	Power down	-07:19:02:46
08/29/2019 14:00:00	Taken off HASP gondola	-06:21:40:00
08/29/2019 14:15:00	Temp Sensors reconfigured	-06:21:25:00
08/29/2019 15:15:00	Attached to HASP gondola	-06:20:25:00
08/29/2019 15:19:06	Begin Overnight Run	-06:20:20:54
08/30/2019 14:24:04	End Overnight Run	-5:21:15:54
09/01/2019 15:30:40	Begin Hang Test	-03:20:09:20
09/01/2019 16:00:00	Command 0x01 0x01 requested	-03:19:40:00
09/01/2019 16:03:39	Command 0x01 0x01 confirmed	-03:19:36:21
09/01/2019 16:09:29	Power Off	-03:19:30:31
09/01/2019 16:31:08	Power On	-03:19:8:52
09/01/2019 16:32:00	Command 0x02 0x01 requested	-03:19:08:00
09/01/2019 16:32:48	Command 0x02 0x01 confirmed	-03:19:07:12
09/01/2019 16:41:23	End Hang Test	-03:18:58:37
09/05/2019 09:02:00	Power On	-00:02:38:00
09/05/2019 09:13:49	Power Off	-00:02:26:11
09/05/2019 09:56:50	Power On	-00:01:43:10
09/05/2019 10:19:59	Power Off	-00:01:20:01
09/05/2019 11:40:00	Power On	00:00:00:00
09/05/2019 13:03:15	Launch	+00:01:23:15
09/05/2019 15:13:00	Power Off	+00:03:33:00
09/05/2019 15:34:00	Power On	+00:03:54:00
09/05/2019 15:40:37	Float Start	+00:04:00:37
09/05/2019 16:11:43	Power Off	+00:04:31:43
09/05/2019 16:12:08	Power On	+00:04:32:08
09/05/2019 23:17:56	Termination	+00:11:37:56
09/05/2019 23:57:03	Impact	+00:12:16:03

Appendix L – SPACER Normalization Data

T (hours at float)	DR1 (Ref Rate)/(Rate)							
	SiPM (1,1)	SiPM (1,2)	SiPM (2,1)	SiPM (2,2)	SiPM (2,3)	SiPM (3,1)	SiPM (3,2)	SiPM (3,3)
0.8038	1	1	1	1	1	1	1	1
1.8041	1.02189866	1.0252737	1.0327865	1.0506946	1.0240178	1.0247048	1.01684024	1.03146369
2.8043	1.04107541	1.044872	1.0587915	1.0940461	1.0512385	1.0499215	1.04166411	1.06122146
3.8046	1.06036594	1.0657758	1.0794099	1.1249796	1.0778561	1.0760637	1.06064201	1.09618978
4.8049	1.06094847	1.0667981	1.0770711	1.1171617	1.0844727	1.0735498	1.06435302	1.09841205
5.8051	1.06506683	1.0733623	1.080864	1.1205833	1.08734	1.0790815	1.07182177	1.11106441
6.8055	1.05446244	1.0577143	1.0626656	1.0956232	1.0763785	1.0666019	1.06004938	1.09374268

Figure 48: Data used to generate the temperature corrections $K_{temp}(t)$ for each SiPM on Data Recorder 1

T (hours at float)	DR2 (Ref Rate)/(Rate)							
	SiPM (1,1)	SiPM (1,2)	SiPM (2,1)	SiPM (2,2)	SiPM (2,3)	SiPM (3,1)	SiPM (3,2)	SiPM (3,3)
0.6559	1	1	1	1	1	1	1	1
1.6563	1.019287694	1.031784	1.0311055	1.0326805	1.0256859	1.0289745	1.03575936	1.02876943
2.566	1.040409678	1.062164	1.0543545	1.0604831	1.0552918	1.0560138	1.0742041	1.06038124
3.6569	1.066108942	1.094431	1.0753105	1.0932139	1.0854699	1.0821885	1.10082211	1.08996663
4.6572	1.068298523	1.099128	1.0769394	1.0978796	1.096514	1.0876114	1.09298908	1.09578517
5.6575	1.081015224	1.104636	1.0806147	1.1064933	1.101902	1.0941611	1.09727037	1.10232174
6.6578	1.061186522	1.091999	1.0563369	1.0930649	1.0887009	1.0729868	1.06667555	1.08836825

Figure 49: Data used to generate the temperature corrections $K_{temp}(t)$ for each SiPM on Data Recorder 1

Data Recorder 1		
SiPM	K-crystal	K-temp (t)
DR1 (1,1)	1.0875	$k(t) = -0.0033t^2 + 0.0345t + 0.9725$
DR1 (1,2)	1.2489	$k(t) = -0.0037t^2 + 0.0384t + 0.9695$
DR1 (2,1)	1.0204	$k(t) = -0.0049t^2 + 0.0481t + 0.9635$
DR1 (2,2)	1	$k(t) = -0.0078t^2 + 0.0754t + 0.9434$
DR1 (2,3)	1.0325	$k(t) = -0.004t^2 + 0.0444t + 0.9625$
DR1 (3,1)	1.3142	$k(t) = -0.0041t^2 + 0.0428t + 0.9651$
DR1 (3,2)	1.0263	$k(t) = -0.0031t^2 + 0.0347t + 0.9701$
DR1 (3,3)	1.0679	$k(t) = -0.0047t^2 + 0.0528t + 0.9562$

Figure 50: SiPM efficiency and temperature corrections for each SiPM on Data Recorder 1

Data Recorder 2		
DR2	K-crystal	K-temp (t)
DR2 (1,1)	1.1394	$k(t) = -0.0035t^2 + 0.0372t + 0.9723$
DR2 (1,2)	1.2487	$k(t) = -0.0049t^2 + 0.0519t + 0.9643$
DR2 (2,1)	1.0203	$k(t) = -0.005t^2 + 0.0468t + 0.9693$
DR2 (2,2)	0.9527	$k(t) = -0.0046t^2 + 0.0505t + 0.9656$
DR2 (2,3)	1.0297	$k(t) = -0.0043t^2 + 0.0478t + 0.9651$
DR2 (3,1)	1.1504	$k(t) = -0.0048t^2 + 0.0485t + 0.9663$
DR2 (3,2)	1.016	$k(t) = -0.0069t^2 + 0.0625t + 0.9584$
DR2 (3,3)	0.9942	$k(t) = -0.0047t^2 + 0.0502t + 0.9648$

Figure 51: SiPM efficiency and temperature corrections for each SiPM on Data Recorder 1